



Integrated multiscale mathematical modeling of insulin secretion reveals the role of islet network integrity for proper oscillatory glucose-dose response



I. Johanna Stamper^a, Xujing Wang^{b,*}

^a The Comprehensive Diabetes Center, University of Alabama at Birmingham, Birmingham, AL 35294, United States

^b The Division of Diabetes, Endocrinology, and Metabolic Diseases (DEM), the National Institute of Diabetes and Digestive and Kidney Diseases (NIDDK), of the National Institutes of Health(NIH), Bethesda, Maryland 20817, United States

ARTICLE INFO

Article history:

Received 20 November 2018

Revised 3 May 2019

Accepted 8 May 2019

Available online 9 May 2019

Keywords:

Insulin secretion

Insulin granule dynamics

Islet cell network

Insulin oscillation

Diabetes

Excitable cell

ABSTRACT

The integrated multiscale mathematical model we present in this paper is built on two of our previous ones: a model of electrical oscillation in β -cells connected to neighboring cells within a three-dimensional (3D) network, and a model of glucose-induced β -cell intracellular insulin granule trafficking and insulin secretion. In order to couple these two models, we assume that the rate at which primed and release-ready insulin granules fuse at the cell membrane increases with the intracellular calcium concentration. Moreover, by assuming that the fraction of free K_{ATP} -channels decreases with increasing glucose concentration, we take into account the effect of glucose dose on membrane potential and, indirectly via the effect on the potential, on intracellular calcium. Numerical analysis of our new model shows that a single step increase in glucose concentration yields the experimentally observed characteristic biphasic insulin release. We find that the biphasic response is typically oscillatory in nature for low and moderate glucose concentrations. The plateau fraction (the time that the β -cells spend in their active firing phase) increases with increasing glucose dose, as does the total insulin secretion. At high glucose concentrations, the oscillations tend to vanish due to a constantly elevated membrane potential of the β -cells. Our results also demonstrate how insulin secretion characteristics in various glucose protocols depend on the degree of β -cell loss, highlighting the potential impact from disease. In particular, both the secretory capacity (average insulin secretion rate per β -cell) and the oscillatory response diminish as the islet cell network becomes compromised.

Published by Elsevier Ltd.

1. Introduction

Glucose homeostasis is a basic physiological process that provides energy to all cells in the body. Dysregulation of this process leads or contributes to a number of common diseases such as diabetes, obesity, and cardiovascular disorders, to name a few. Insulin, which is secreted by the pancreatic islet β -cells, is the primary regulating hormone of glucose homeostasis. A quantitative understanding of key factors that control insulin secretion, and the major components of its action, is thus an important research objective.

In the past several decades, numerous mathematical models have been developed to explore various aspects of β -cell function. Mathematical modeling, in conjunction with laboratory investigations, has for example attributed oscillatory insulin secretion

to glucose-stimulated oscillations in the β -cells' electrical activity (Chay and Keizer, 1983; MacDonald et al., 2005; Marinelli et al., 2018; McKenna et al., 2016a, 2016b; Pedersen, 2009; Pedersen et al., 2005; Rorsman and Renstrom, 2003; Wang and Thurmond, 2009). The variations in β -cell membrane potential and intracellular calcium, (which, when elevated, triggers calcium-dependent exocytosis of insulin granules) translate into bursts of insulin release interspersed by secretory pauses. As insulin is secreted from the pancreas in pulsatile fashion, oscillations in blood insulin and blood glucose are also established. The regular temporal variations in peripheral blood-borne insulin are believed to be an important part in keeping glucose concentrations within a healthy range. Indeed, pulsatile insulin levels have been shown to be more effective at lowering glucose than constant levels (Bratusch-Marrain et al., 1986; Matthews et al., 1983). Impaired or completely lost insulin oscillation affects both diabetic patients and their relatives (O'Rahilly et al., 1988; Schmitz et al., 1997; Zarkovic et al., 1999). In intact pancreatic islets, β -cells are electrically coupled to each other via gap junctions, membrane channels which allow for ionic

* Corresponding author.

E-mail addresses: johannastamper@rocketmail.com (I.J. Stamper), xujing.wang@nih.gov (X. Wang).

and molecular exchanges between neighboring cells. Both mathematical models and experimental observation indicate that such coupling enables the β -cells to synchronize their oscillatory response, thereby establishing coordinated insulin pulsatility (Head et al., 2012; Meda, 2012; Ravier et al., 2005; Sherman and Rinzel, 1991; Sherman et al., 1988; Smolen et al., 1993).

Other areas frequently subject to mathematical modeling include intracellular insulin granule trafficking and the glucose-dose-dependent insulin secretion observed during various glucose protocols. Inside a pancreatic islet β -cell, insulin granules are stored in several distinct pools. Upon a step increase in glucose concentration, a biphasic response within the first ~30–60 min is expected, featuring an initial insulin spike followed by a slowly increasing secretion phase. Since it was first observed (Curry et al., 1968), biphasic secretion has been detected from islets and pancreata of both human and rodent origins (Fujimoto et al., 2000; Grodsky, 1972; Henquin et al., 2006; Straub and Sharp, 2002; Straub et al., 2004), and it has been noted that Type 2 diabetes is associated with a severely reduced first phase (Nagamatsu et al., 2006; Ohara-Imazumi et al., 2004; Rorsman and Renstrom, 2003). Mathematical models have been successful in reproducing the biphasic secretion patterns (Bertuzzi et al., 2007; Chen et al., 2008; Pedersen and Sherman, 2009; Pedersen et al., 2008; Stamper and Wang, 2013). Model analysis has also offered insight into more complex secretion patterns. For example, involving glucose staircase protocols, models assuming either heterogeneous glucose-activated insulin secretion within a population of β -cells (Grodsky, 1972; Pedersen et al., 2008) or a graded glucose-dose-response of individual β -cells (Stamper and Wang, 2013) have been put forward to explain the insulin spikes of increasing heights observed as the glucose concentration is increased in a series of steps.

Despite these research efforts, there are still several outstanding gaps that need to be filled before we can achieve a comprehensive and quantitative understanding of glucose-stimulated insulin secretion. Identification of key factors determining the amount of insulin released and its temporal variations are of particular interest. In this paper we aim to shed light on some of these aspects with a special focus on how the rate and the total amount of insulin secretion, and the establishment of oscillations in the secretion, are altered by varying degree of β -cell loss and compromised pancreatic islet architectural integrity, abnormalities contributing to the development of both human Type 1 and Type 2 diabetes (Kilimnik et al., 2011; Morgan et al., 2014). The glucose protocols that we study here include the step increase from basal, as well as the potentiation, the ramp and the staircase experiments.

The mathematical model that we develop in this paper builds on our previous models of insulin granule pool dynamics (Stamper and Wang, 2013), and of islet β -cell network electrophysiology (Nittala and Wang, 2008; Nittala et al., 2007). In the granule pool model we considered the islet β -cells as a collection of identical cells in which granule fusion was directly dependent on the extracellular glucose concentration (Stamper and Wang, 2013). In the islet model we studied how cell network structure affects β -cell electric activity by describing an islet as a three-dimensional hexagonally closest packed (3D HCP) network of heterogeneous β -cells electrically coupled to their nearest neighbors (Nittala and Wang, 2008; Nittala et al., 2007). Here we integrate the two models, and further connect insulin secretion via trafficking of intracellular insulin granules to changing intracellular calcium levels affected by glucose-induced changes in both membrane electric potential and conductance of the K_{ATP} -channel, thus linking changes in β -cell electrical activity and insulin secretion rate to variations in extracellular glucose concentration. Such a glucose effect is consistent with experimental observations. For example, in Ren et al. (2013) it was reported that the conductance of the

K_{ATP} -channel was high at low glucose (2.8 mM) due to many open channels and low at high glucose (11.1 mM).

By integrated modeling of both the β -cell's intracellular granule pools and its electrophysiology, we are able to account for insulin's oscillatory nature. By applying our model to clusters of electrically coupled β -cells, we can study directly how islet network connectivity influences the insulin secretion rate and its temporal characteristics. Recently Notary et al. (2016) developed a model that combines a granule pool model (Pedersen and Sherman, 2009) with an electrophysiological model of β -cells arranged in a random sphere-packing architecture (Hraha et al., 2014). Interestingly, their model was able to recreate oscillatory biphasic insulin secretion after a step increase in the glucose concentration. However, the focus of their study was the role of gap-junctional coupling in insulin secretion, and how it is affected by ATP-insensitive K_{ATP} -channels in neonatal diabetes mellitus; the role of varying structure of the β -cell network was not considered.

The rest of our paper is organized as follows. In the next section we present our new model, in which the evolution of key variables for each individual islet β -cell is given by a system consisting of coupled nonlinear ordinary differential equations (ODEs). In Section 3 we analyze the response of various islets to different glucose protocols. Finally, a discussion of our results is contained in Section 4.

2. Model development

Fig. 1 presents the overall scheme of our integrated mathematical model. At the center of the picture are two intracellular pathways stimulated by an elevated extracellular glucose level: the membrane depolarization and electric oscillation pathway (depicted on the left side of the β -cell interior); and the insulin granule dynamics and secretion pathway (depicted on the right side).

Influx of glucose into the β -cells occurs via special glucose transporters located at the cell surface (MacDonald et al., 2005; Rorsman and Renstrom, 2003; Wang and Thurmond, 2009). Subsequent metabolism increases the ATP/ADP ratio, causing ATP-dependent K^+ -channels in the plasma membrane to close. When glucose is elevated above basal, the closure of sufficiently many channels depolarizes the cell membrane, thereby increasing the membrane potential from its resting potential of about -70 mV. Depolarization leads to the opening of voltage-dependent Ca^{2+} -channels and influx of Ca^{2+} (MacDonald et al., 2005; Rorsman and Renstrom, 2003; Wang and Thurmond, 2009). The rise in intracellular Ca^{2+} induces exocytosis of insulin granules via granule fusion with the plasma membrane. Only a subset of all insulin granules, the release-ready, so-called primed granules, are able to undergo fusion. Refilling of the readily releasable granule pool occurs via a number of glucose-dependent reactions (Rorsman and Renstrom, 2003; Wang and Thurmond, 2009), involving movement/mobilization of granules from the cell interior, remodeling of filamentous actin and chemical reactions, e.g. ATP-dependent granular acidification (Barg et al., 2001; Wang and Thurmond, 2009). Each insulin-secreting β -cell does not function alone. Indeed, the β -cell mass is organized in a hierarchical fashion with β -cells residing in pancreatic islets rather than being dispersed uniformly across the pancreas. Inside each islet the β -cells are electrically coupled to each other. The structure of the β -cell network plays an important role in modulating both the amount and the oscillatory characteristics of the insulin being secreted (Nittala and Wang, 2008; Nittala et al., 2007).

In Section 2.1 we model glucose-dependent changes in membrane potential and intracellular calcium, i.e., the left intracellular pathway in Fig. 1, by modifying a Hodgkin-Huxley (H-H) type model developed in Nittala and Wang (2008) and Nittala et al. (2007). To model the evolution of the various pools of

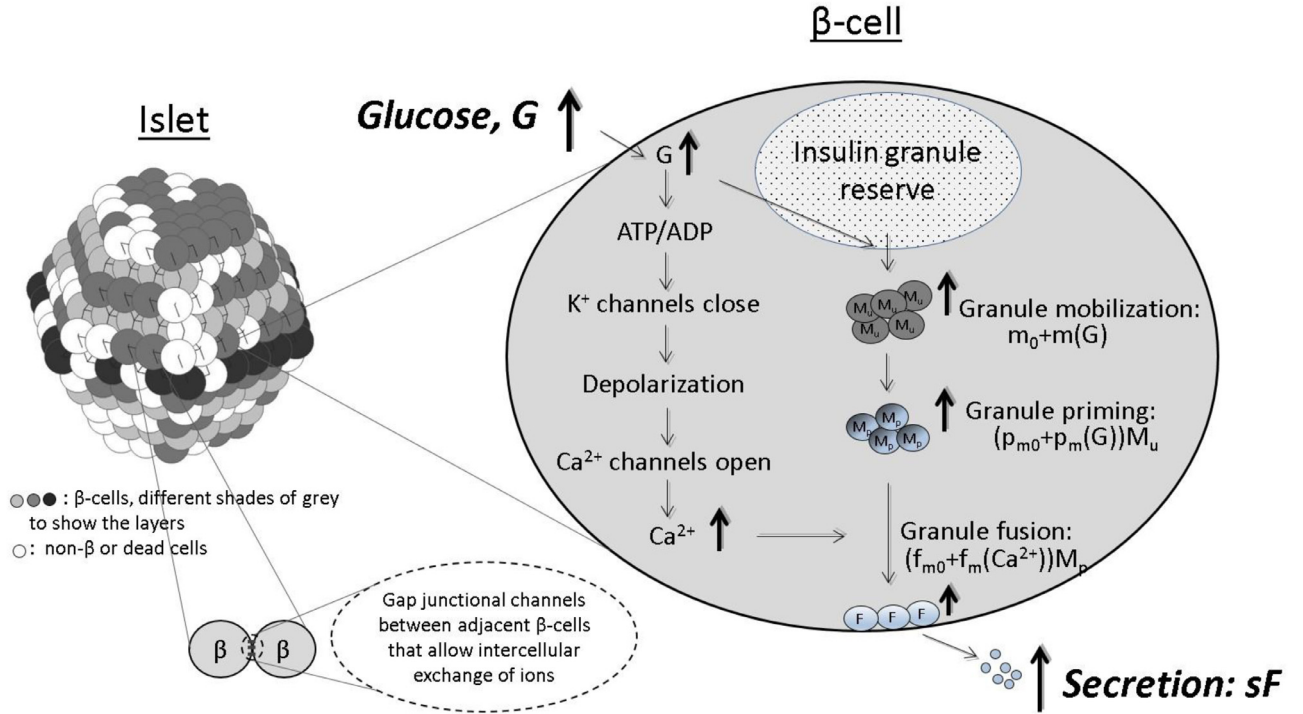


Fig. 1. Schematic diagram of our integrated multiscale mathematical model. Left: An islet with 587 cells packed in Hexagonal Closest Packing (HCP) lattice structure. Cells in different layers of the network are colored with different shades of grey to show the packing structure. Bottom: Two adjacent islet β -cells are electrically coupled to each other through gap-junctional channels, allowing for transfer of ions and small molecules between them. Right: The intracellular granule model in which insulin secretion occurs via calcium-facilitated granule fusion and exocytosis, following glucose-stimulated mobilization and priming of granules from the reserve pool. The rates at which granules are transferred between the different granule pools and being secreted from the fused pool are shown next to the arrows.

intracellular insulin granules and calcium-dependent insulin secretion, *i.e.*, the right intracellular pathway in Fig. 1, in Section 2.2 we modify a model that we previously developed and analyzed in Stamper and Wang (2013). In Section 2.3 we describe how the β -cells are situated in a network and how the functional role of β -cell coupling structure will be numerically investigated. State variables and parameters of the new integrated model are summarized in Appendix A, Tables A1 and A2, respectively.

2.1. H-H type model for the evolution of membrane potential and intracellular calcium in electrically coupled β -cells

In what follows we use the subscript i to denote variables and parameters that are specific to β -cell i . Along the pathway depicted on the left side of the β -cell interior in Fig. 1, the rate of change in membrane potential, V_i , and in intracellular calcium concentration, $[\text{Ca}^{2+}]_i$, of β -cell i are given by the following two ODEs, respectively, as previously described (Nittala and Wang, 2008; Nittala et al., 2007):

$$C_m \frac{dV_i}{dt} = -\left(I_{\text{Ca},i} + I_{K_{\text{ATP}},i} + I_{K,i} + I_{S,i}\right) - \sum_{j \in \text{all cells coupled to } i} g_c(V_i - V_j), \quad (1)$$

and

$$\frac{d[\text{Ca}^{2+}]_i}{dt} = -f(\alpha_i I_{\text{Ca},i} + k_{\text{Ca},i} [\text{Ca}^{2+}]_i), \quad (2)$$

where C_m , g_c , f , α_i , $k_{\text{Ca},i}$ are positive constants (Table A2). The ion current terms are given by:

$$I_{\text{Ca},i} = g_{\text{Ca}} m_\infty (V_i - V_{\text{Ca}}) \quad (3)$$

$$I_{K_{\text{ATP}},i} = g_{K_{\text{ATP}}} O_{K_{\text{ATP}}} (V_i - V_K) \quad (4)$$

$$I_{K,i} = g_K n_i (V_i - V_K) \quad (5)$$

$$I_{S,i} = g_S s_i (V_i - V_K) \quad (6)$$

with constants g_{Ca} , $g_{K_{\text{ATP}}}$, g_K , g_S , V_{Ca} and V_K (Table A2). Furthermore,

$$\frac{dn_i}{dt} = \frac{(n_\infty(V_i) - n_i)}{\tau_n} \quad (7)$$

$$\frac{ds_i}{dt} = \frac{(s_\infty(V_i) - s_i)}{\tau_s} \quad (8)$$

where τ_n and τ_s are time constants (Table A2), and

$$x_\infty(V_i) = \frac{1}{1 + \exp((V_x - V_i)/\theta_x)} \quad (9)$$

with constants V_x and θ_x for $x = m, n, s$ (Table A2). In contrast to the previous model (Nittala and Wang, 2008; Nittala et al., 2007) where $O_{K_{\text{ATP}}}$, the fraction of free K_{ATP} -channels, was a constant ($O_{K_{\text{ATP}}} \in [0, 1]$), here we assume that $O_{K_{\text{ATP}}}$ is glucose-dependent:

$$O_{K_{\text{ATP}}} = \frac{1}{1 + (G/G_{K_{\text{ATP}},50})^\gamma} \quad (10)$$

where G is the glucose concentration and $G_{K_{\text{ATP}},50}$ is the glucose concentration at which the conductance is half-maximal, and γ is a positive constant. The total conductance of the K_{ATP} -channel is given by $g_{K_{\text{ATP}}} O_{K_{\text{ATP}}}$, where $g_{K_{\text{ATP}}}$ is the maximum conductance. Thus the effect of increasing the glucose concentration is to lower the number of free K_{ATP} -channels, thereby lowering the K_{ATP} -channel conductance.

We note that in Eq. (1), for simplicity and to focus on the integration of modeling across multiple scales, we assume a uniform gap junctional coupling strength of 200 pS in each islet (Table A2). Additionally, the effect on intracellular calcium from gap-junctional

coupling is probably small due to the relatively small concentration of calcium ions compared to K^+ and Na^+ ; hence, in accordance with the model in Smolen et al. (1993), we do not include a term for gap-junctional coupling in Eq. (2). Lastly, we remark that we, for simplicity, refrain from modeling ATP and ADP explicitly. In our model, bursting is completely dependent on the voltage-dependent $I_{S,i}$ -current. This minimal modeling approach gives rise to relaxation oscillations and has previously been utilized in Sherman (1996). When other mechanisms for bursting, e.g. calcium and ATP-dependent ones, are included, a wider range of oscillation types emerges, as for example discussed in Marinelli et al. (2018).

2.2. Model of β -cell intracellular insulin granule dynamics and insulin secretion

The intracellular granule component, depicted on the right side of the β -cell interior in Fig. 1, is a simplified and modified version of the model we previously developed in Stamper and Wang (2013). In the original model the intracellular insulin granules were divided into five subgroups (Stamper and Wang, 2013): mobilized unprimed granules, $M_u(t)$; mobilized primed granules, $M_p(t)$, docked unprimed granules, $D_u(t)$, docked primed granules, $D_p(t)$, and fused granules, $F(t)$. Here we merge the docked pools $D_u(t)$ and $D_p(t)$ into the corresponding mobilized pools $M_u(t)$ and $M_p(t)$, thus reducing the number of subpools to three (Fig. 1, β -cell panel, right side). This simplification gives comparable secretion patterns as the original model. A similar three-pool model of granule trafficking has also been reported by others (Pedersen et al., 2008). Additionally, we set all time delays in the glucose-dependent rate constants to zero ($\delta_m = \delta_p = \delta_f = 0$). This simplification does not change the major characteristics of the system response, apart from not shifting the response a certain number of units of time. Finally, the fusion rate is assumed to be dependent on the intracellular calcium level (versus directly on glucose as assumed in the previous model (Stamper and Wang, 2013)). We remark that while the rate of fusion is now calcium-dependent, we keep the rates for mobilization and priming dependent on glucose. If ATP and ADP were explicitly modeled, we could make mobilization and priming ATP-dependent. We anticipate that such a modeling approach would mainly introduce a brief time delay in mobilization and priming. In addition, if ATP levels are oscillatory (Ren et al., 2013), additional oscillations could be introduced into the granule dynamics.

With the above changes, insulin secretion from each β -cell is now modeled via the following three equations:

$$\dot{M}_{u,i} = \underbrace{m_0 + \hat{m}(t)}_{\text{mobilization}} - \underbrace{(p_{m0} + \hat{p}_m(t))M_{u,i}}_{\text{priming}}, \quad (11)$$

$$\dot{M}_{p,i} = \underbrace{(p_{m0} + \hat{p}_m(t))M_{u,i}}_{\text{priming}} - \underbrace{(f_{m0} + \hat{f}_m(t))M_{p,i}}_{\text{fusion}}, \quad (12)$$

$$\dot{F}_i = \underbrace{(f_{m0} + \hat{f}_m(t))M_{p,i}}_{\text{fusion}} - \underbrace{sF_i}_{\text{secretion}}, \quad (13)$$

where m_0 , p_{m0} , f_{m0} and s are constant basal rates (Table A2), $\hat{m}(t)$ and $\hat{p}_m(t)$ are glucose-dependent and $\hat{f}_m(t)$ is dependent on the intracellular calcium level. In particular,

$$\hat{m}(t) = \tilde{m}(t) \left(1 - \frac{M_{u,i}}{M_{u,max}} \right) \quad (14)$$

where $M_{u,max}$ is a positive constant and

$$\tilde{m}(t) = \frac{m[G(t) - G_m]^{\kappa_m}}{[G_{m50} - G_m]^{\kappa_m} + [G(t) - G_m]^{\kappa_m}} H(G(t) - G_m), \quad (15)$$

κ_m is a Hill coefficient, m is the maximal rate of stimulated mobilization, G_{m50} is the level of extracellular glucose at which \tilde{m} is half-maximal, and $H(x)$ is the Heaviside step function ($H(x) = 0$ if $x < 0$, and $H(x) = 1$ if $x \geq 0$), so that glucose-induced mobilization occurs when the concentration of glucose is above the threshold, G_m . Similarly, when the glucose level is above G_p enhanced priming takes place with rate coefficient $\hat{p}_m(t)$ given by:

$$\hat{p}_m(t) = \frac{p_m[G(t) - G_p]^{\kappa_p}}{[G_{p50} - G_p]^{\kappa_p} + [G(t) - G_p]^{\kappa_p}} H(G(t) - G_p), \quad (16)$$

where p_m is the maximum rate and G_{p50} is the level of glucose at which the rate of priming is half-maximal. For the fusion rate coefficient we assume the following form:

$$\hat{f}_m(t) = \frac{f_m [[Ca^{2+}]_i(t) - Ca_f]^{\kappa_f}}{[Ca_{f50} - Ca_f]^{\kappa_f} + [[Ca^{2+}]_i(t) - Ca_f]^{\kappa_f}} H([Ca^{2+}]_i(t) - Ca_f), \quad (17)$$

where Ca_{f50} is the level of intracellular calcium at which the calcium-dependent rate of fusion of primed mobilized granules is half-maximal, $f_m/2$, and Ca_f is the activation threshold.

The number of granules secreted by a single β -cell per unit time is given by sF_i for cell i , and is expected to vary from cell to cell due to heterogeneity. The total insulin secretion rate for an islet, $I(t)$, is given by:

$$I(t) = \sum_{i=1}^{N_\beta} I_g s F_i(t), \quad (18)$$

where I_g is the insulin content of one granule and N_β is the number of β -cells in the islet. In order to be able to compare the insulin secretion capacity for islets of different size and composition, we also calculate the mean insulin secretion per cell, $I_{cell}(t)$, as $I_{cell}(t) = I(t)/N_\beta$. When simulating an experimental protocol (step increase, staircase, etc.) we determine the total amount of insulin secreted, J , given by the area under the $I(t)$ curve as defined by the Trapezoid Rule:

$$J = \frac{\Delta t}{2} \left(I_0 + \sum_{i=1}^{n-1} I_i + I_n \right), \quad (19)$$

where $I_i = I(t_i)$, $t_i = i\Delta t$, $i = 0, \dots, n$ and $\Delta t = T/n$ with T being the length of time of the simulated experimental protocol. In this study $\Delta t = 0.01$ min, $T=10$ min. The total insulin secretion per cell, J_{cell} , is defined as $J_{cell} = J/N_\beta$.

2.3. Islet configurations and numerical simulations

In this study, we simulate islets whose cells are arranged in a three-dimensional hexagonally closest packed (3D HCP) network. Each functional β -cell is modeled via its own set of the seven ODEs, (1)–(2), (7)–(8) and (11–13), above. We solve the resulting system of equations numerically by using MATLAB's ODE solver ode45. In the remainder of this paper, unless otherwise stated, we present simulation results obtained from islets with 587 cells (Fig. 1, top left panel). This is in the range of normal, human islets which typically may contain a few hundred cells up to a few thousand cells (Ahren et al., 2010; Pisania et al., 2010; Smelt et al., 2008). The actual number of β -cells in each islet varies due to the presence of other cell types (Pisania et al., 2010; Smelt et al., 2008), primarily the glucagon- and somatostatin-secreting α -cells and δ -cells, and due to cell death from disease (Rhodes, 2005). Experimental studies typically estimate the proportion of β -cells to $\sim 50\text{--}80\%$ in normal healthy human islets (Cabrera et al., 2006). Clinical observations have found that up to 70–90% of the β -cells may be lost during development of a disease like Type 1 Diabetes

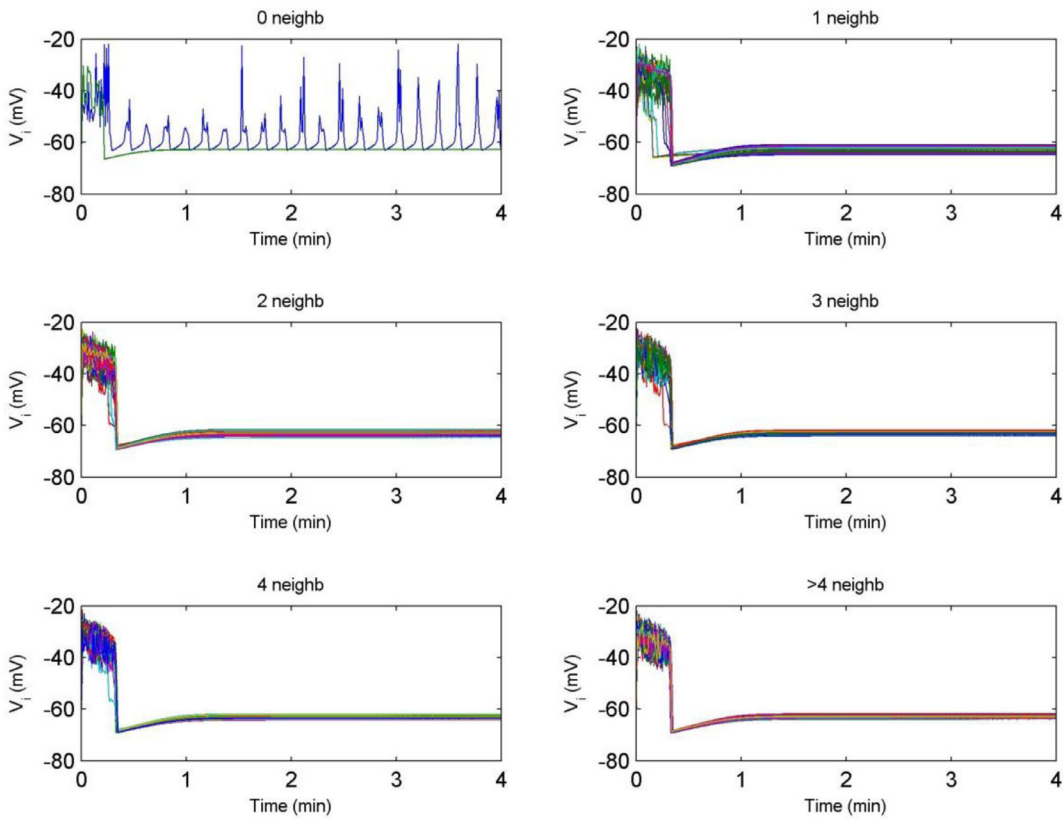


Fig. 2. At basal glucose level few β -cells are active in islets with a high fraction of functional β -cells. Panels show electrical activity of all individual β -cells from a total of six simulated islets of size 587, in which half of the cells are functional β -cells ($F_\beta = 0.5$). Only two β -cells have no coupling neighbors, and one of these cells is the only active cell (top left panel). All other cells have at least one coupling neighbor, and are electrically silent at basal. Parameter values are given in Table A2 column 3 with $G = 2.8 \text{ mM}$.

before disease onset (Gepts, 1965; van Belle et al., 2011). While we in this paper disregard modeling α -cells and δ -cells and focus on β -cells exclusively, we do simulate islets with a varying fraction of functional β -cells, F_β , ranging from 0.9 (for largely intact islets) to 0.1 (for highly disintegrated islets). Each simulation starts by randomly assigning a certain percentage of the islet's cells as non-functional or non- β . These cells do not couple with functional β -cells, and the sites containing such cells do not contribute in any way to the simulation of functional β -cells. To obtain different β -cell network configurations of the same F_β , we initialize MATLAB's random number generator with different values (so-called random seeds). In general we simulate each F_β with six different random seeds (using the same set of six seeds for every F_β). Within each of the six resulting islet configurations we implement cell heterogeneity following a normal distribution for the parameters g_{Ca} , g_K , $g_{K_{ATP}}$, g_s , k_{Ca} , α and C_m , as previously (Nittala et al., 2007). For each of these parameters we assume that the standard deviation is five percent of the mean value. For more on model variables and parameters we refer the reader to Tables A1 and A2 in the Appendix where variables and parameters are given along with their units and value ranges.

3. Results

In all numerical simulations we first allow the islet to settle to its basal steady state, before applying any glucose protocols. In Section 3.1 we investigate characteristics of basal secretion. In Section 3.2 we study the model's response to single glucose steps of varying concentrations. Due to its relative simplicity, we use the step glucose protocol for major analysis of various topics of interest, including oscillatory response, total insulin secretion (area

under the curve), glucose-dose-dependency, total intracellular calcium and plateau fraction. Finally, in Sections 3.3–3.5 we show how our model can reproduce additional experimental glucose protocols and observations, namely potentiation, ramp and staircase.

3.1. Heterogeneity in basal secretion

The initial conditions used for the basal simulation are as follows for all β -cells: $V(0) = 65 \text{ mV}$, $[Ca^{2+}](0) = 0.07 \mu\text{mol/l}$, $n(0) = 0.15 \text{ ms}^{-1}$, $s(0) = 0.03 \text{ ms}^{-1}$, $M_u(0) = 250$, $M_p(0) = 25/0.8$ and $F(0) = 1/30$. In Fig. 2 we show the responses of all cells from six islets with $F_\beta = 0.5$, while those from six islets with $F_\beta = 0.1$ are presented in Fig. 3. We show only the first 4 min of simulations as within this time frame all cells reached stable patterns which represent the cells' basal states. We sort the basal insulin secretion patterns of β -cells based on the number of nearest neighbors each cell has. Evidently, the likelihood of cell activation (with active cells defined as cells showing an active firing phase with voltage level above -50 mV), decreases as the number of nearest neighbors increases. Typically the basal state of islets with a low β -cell fraction ($F_\beta = 0.1$ or $F_\beta = 0.3$) contain some active cells (8 out of 12 simulated) whereas most islets (17 out of 18 simulated) with an intermediate or high degree of β -cells ($F_\beta = 0.5$, $F_\beta = 0.7$ or $F_\beta = 0.9$) evolve to a totally quiescent basal steady state.

In Figs. 2 and 3, top left panels, we note that β -cells with no coupling partners may be inactive or active (due to cellular heterogeneity). Cells that would be inactive in the absence of nearest-neighbor peers exert, when coupled, hyperpolarizing currents on their more excitable neighbors (the g_c -term in Eq. (1)) (Benninger et al., 2011). If these currents are sufficiently strong, the

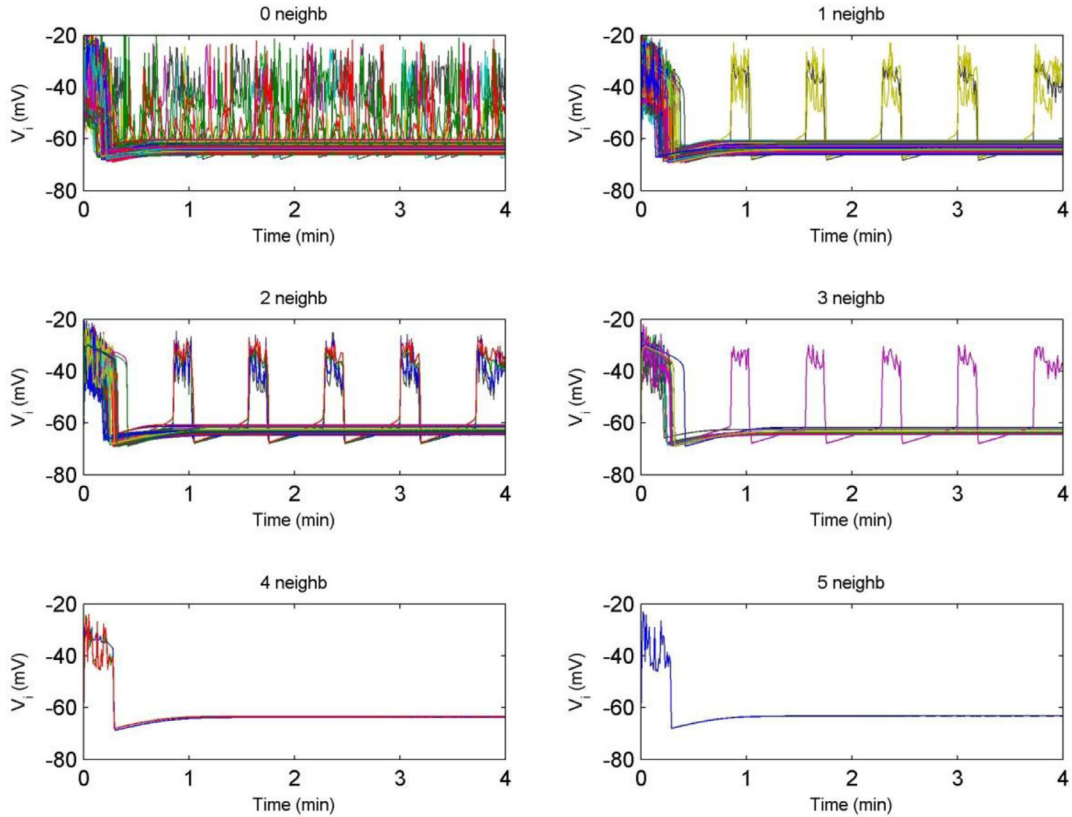


Fig. 3. In islets with a low fraction of functional β -cells a significant number of cells are electrically active even at the basal glucose level, and β -cell electrical activity varies depending on the number of coupled nearest neighbors. Results shown are from a total of six simulated islets of size 587, in which ten percent of the cells are functional β -cells ($F_\beta = 0.1$). Those with less than four nearest neighbors may be active at basal glucose. Parameter values are as in Fig. 2, and are given in Table A2 column 3 with $G = 2.8$ mM.

islet as a whole stays inactive. As seen in Eq. (1), the strength of the hyperpolarizing current depends on both the number of cells connected as well as on their membrane potential differences. This means that the effect of having a certain number of coupled neighbors may be different between different islets. Indeed, comparing Figs. 2 and 3, we note that the likelihood of cell activation for cells with either one, two or three nearest neighbors is lower in islets with $F_\beta = 0.5$ than it is in islets with $F_\beta = 0.1$. This is due to the difference in islet structural configuration and one possible explanation is the percolation of the islet beta cell network, as we previously described (Stamper et al., 2014). In islets with a higher F_β value, each β -cell is more likely to be in a larger network of connected β -cells, even when the cell itself has a very low number of viable nearest neighbors.

In the following Sections 3.2–3.5 of this paper, before the start of any glucose stimulation protocol the β -cells were first initialized for 4 min (−4 min to 0 min) at a basal glucose level (2.8 mM) to bring the system to its steady basal state.

3.2. Single step glucose increase

In response to a step increase in the glucose concentration, our new model presented in Fig. 1 produces a biphasic insulin secretion profile with an initial spike followed by a slowly increasing secretion (results not shown, but see Fig. 9 where the secretion during the first step increase on glucose is biphasic), as we previously noted in simulations with a five-pool model of insulin granules (see Fig. 2 of (Stamper and Wang, 2013)), and as noted in multiple experiments (Fujimoto et al., 2000; Grodsky, 1972; Straub and Sharp, 2002; Straub et al., 2004).

Examination of individual cells in islets reveals a significant impact of intercellular coupling and islet structural conformation on β -cell electrical activity and synchronization. Fig. 4 shows the electrical responses of cells from two typical islets with different amounts of β -cell loss to varying step increases of the glucose concentration applied at $t = 0$ min. If the fraction of functional β -cells is high (left panels), then the cells synchronize their response. At low glucose the entire cell population stays electrically silent. As the glucose concentration is increased, the cells start bursting. As has been noted in other mathematical models and experimentally (Miura and Pernarowski, 1995; Nunemaker et al., 2006b; Smolen et al., 1993), the plateau fraction, i.e. the fraction of time that the β -cells spend in the active firing phase, increases with increasing glucose dose. As glucose is increased further, the cells change from being bursting to spiking cells, which fire constantly and asynchronously (the membrane potential stays elevated at all times). This is also a normal response, consistent with previous reports of β -cells' firing constantly when the glucose concentration reaches above a certain threshold (Kanno et al., 2002).

In contrast, in an islet that has suffered extensive β -cell loss (Fig. 4, right panels) the glucose-dose-dependency in the electrical response is very different. Even at very low glucose a subset of the cells is active, while at intermediate and high glucose some of the cells remain inactive. Compared to structurally intact islets, in which the secretory response switches on/off as the glucose concentration crosses its basal concentration threshold, in disintegrated islets the response is more blunted, as have been noted experimentally as well (Heart et al., 2006; Jonkers and Henquin, 2001; Speier et al., 2007a). Overall, the islet β -cells respond heterogeneously, displaying a mix of silent, bursting, and spiking cells, which also causes the oscillatory response to be less robust for

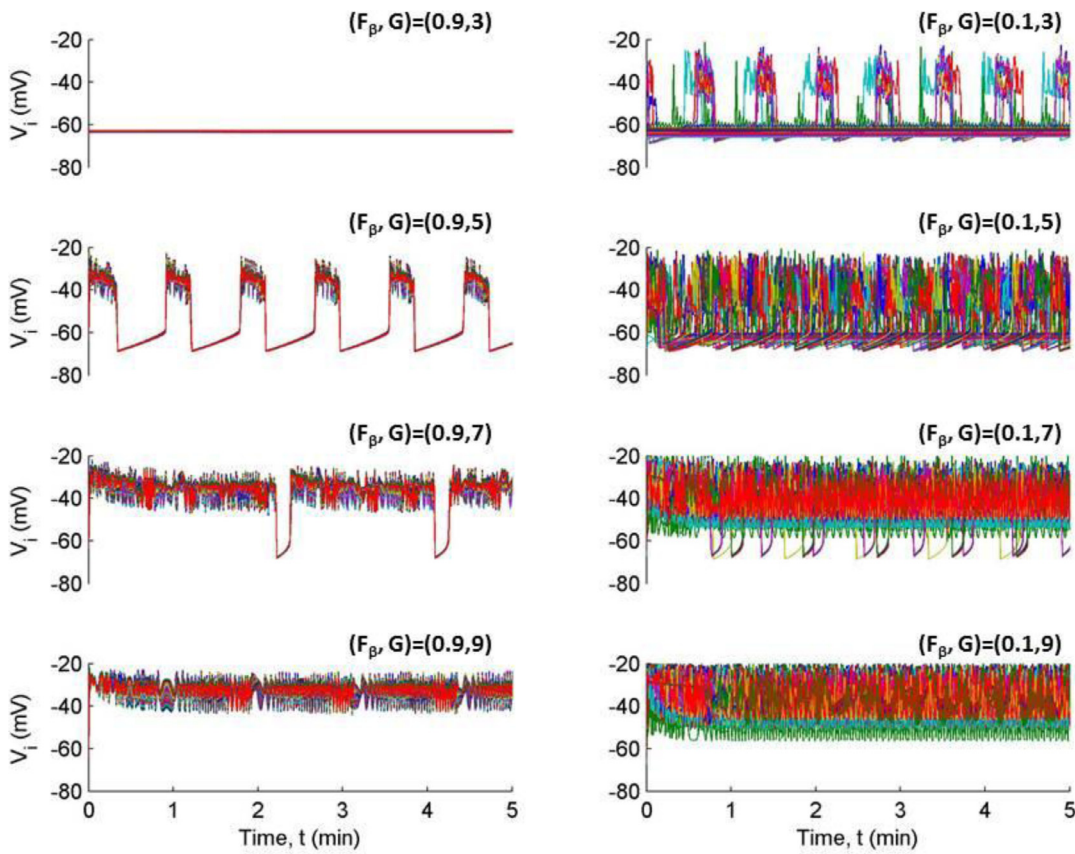


Fig. 4. Comparison of electrical oscillation patterns at different glucose levels of all β -cells from an islet with a high ($F_\beta = 0.9$, left panel) versus a low ($F_\beta = 0.1$, right panel) fraction of functional β -cells. Left: The electrical response is synchronized. Cells are inactive at low glucose (top), and fire constantly at high glucose (bottom). For intermediate glucose concentrations (middle two panels), the plateau fraction increases with increasing glucose concentration. Right: Even at low glucose some of the cells are active. The electrical response of the cells is unsynchronized. The cell population is a mix of bursting, spiking and silent cells. Parameter values as in Fig. 2, with varying F_β and G . The unit for the glucose doses is mM.

intermediate glucose doses. We remark that the membrane potential can be analyzed for single, unconnected cells ($g_c = 0$) as described in Appendix B and Figs. A1–A2. The cells' behavior observed here in a disintegrated islet (Fig. 4, right panels) is similar to that of single, unconnected cells described in Appendix B.

We now examine the insulin secretion rate. When oscillations are present in the membrane potential, since the membrane depolarization will trigger action potential firing and opening of the voltage-dependent Ca^{2+} channels, the intracellular calcium concentration also oscillates. Since the insulin secretion rate depends on the rates of exocytosis and fusion, which in turn depend on the intracellular calcium concentration, the oscillations in the calcium level ultimately lead to oscillations in the insulin secretion rate. We also refer the readers to additional reports on biphasic and oscillatory insulin secretion in experimental settings (Bergsten and Hellman, 1993; Curry et al., 1968; Dishinger et al., 2009; Nuneemaker et al., 2006a; Rorsman et al., 2000). In Fig. 5 we present the per cell insulin secretion rates of the two islets in Fig. 4. With the exception of the lowest glucose dose, the oscillations in the insulin secretion rate are more pronounced and regular for the islet with a low degree of β -cell loss. Irrespective of the amount of β -cell loss, we note that the oscillations become suppressed at the highest glucose dose where cells enter into their constantly spiking mode (bottom panels of Fig. 4, bottom right panel of Fig. 5). In this case, since the membrane potential stays elevated, the oscillations in the calcium level (and thus in the rate of secretion) are relatively small. In Appendix C we show additional plots (Figs. A3–A5) of the insulin secretion rate in islets that have varying degree of β -cell loss, initialized with different random seeds.

In Fig. 6 we show the mean total insulin secretion (area under the curve) during the first phase (first ten minutes) of different elevations of glucose concentration applied as a step increase at time $t = 0$. Glucose dose dependent response is evident: both the total and the per cell total insulin secretion increase with higher glucose concentrations. We note that the per cell total insulin secretion at intermediate and high glucose doses (bottom panel) for the islets with ninety percent β -cell loss ($F_\beta = 0.1$) is markedly lower than for the other islets, but elevated at the lowest (basal) glucose concentration (Fig. 6, inset). Experimental studies have shown similar effects; loss of β -cell coupling increases basal insulin release (Speier et al., 2007a). In Fig. 7 we quantitatively show how the steepness of the dose response curves in Fig. 6 changes with F_β , the fraction of functional cells. It is evident that the sensitivity to glucose dose elevation, as reflected from the increase in total insulin secretion compared to the amount secreted at basal ($G = 3 \text{ mM}$), improves rapidly by increasing the fraction of functional β -cells when F_β low, up till $F_\beta \sim 0.5$, at which point the improvement plateaus. This result indicates that there is more or less a “secretory on/off switch” as F_β is increased beyond some threshold value, around 0.5 (50%); this result echoes our findings in Stamper et al. (2014) where we studied islet oscillation from the perspective of network percolation.

In Fig. 8 we further examine the mechanism of glucose dose response, and the difference between islets with a high and a low β -cell fraction. It is known that elevated glucose raises the rate of insulin release through increasing the average intracellular calcium concentration, since the latter triggers the exocytosis of intracellular insulin granules from β -cells (Ashcroft and Rorsman, 1989).

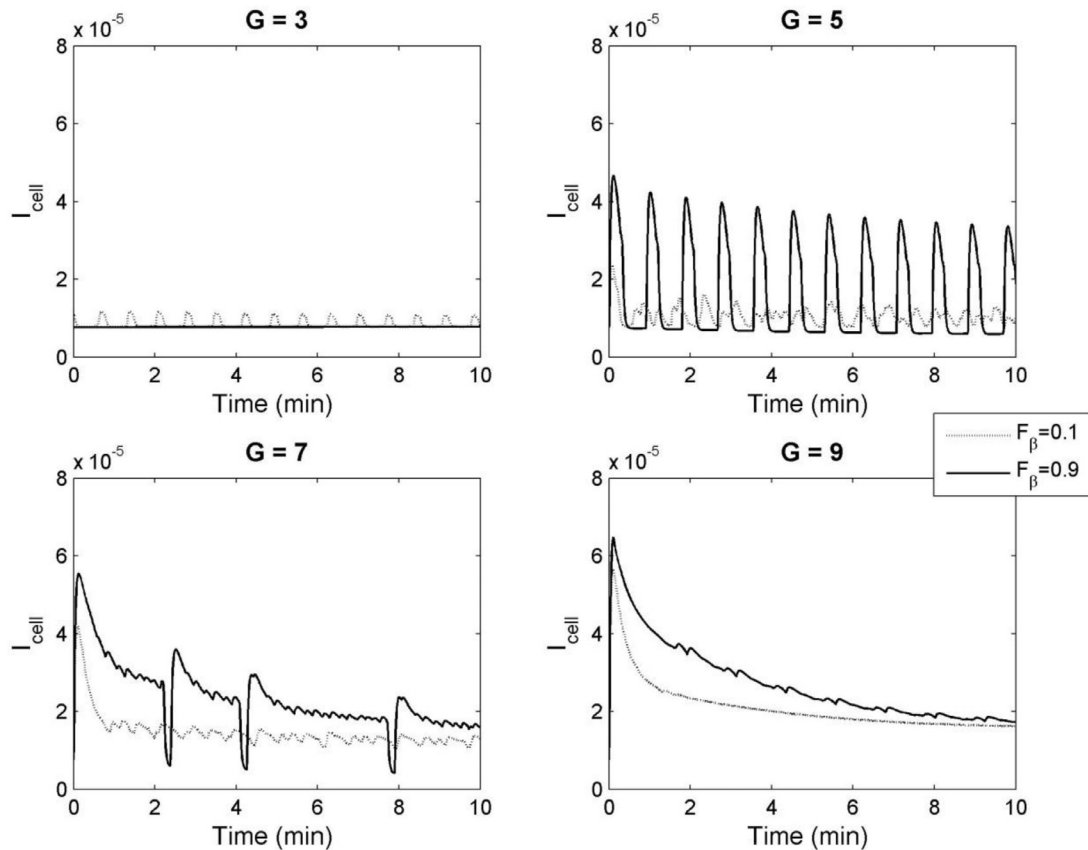


Fig. 5. Oscillation in glucose-induced insulin secretion rate depends on β -cell loss. Four panels showing per-cell insulin secretion rate, $I_{cell}(t)$, for four different glucose concentrations in an islet with either a low amount of β -cell loss (solid lines, $F_\beta = 0.9$) or a high amount of β -cell loss (dashed lines, $F_\beta = 0.1$). With the exception of the lowest glucose case, oscillations in the insulin secretion rate are damped both by β -cell loss and by high glucose. Parameter values are given in Table A2 column 3. The glucose doses are in the unit of mM.

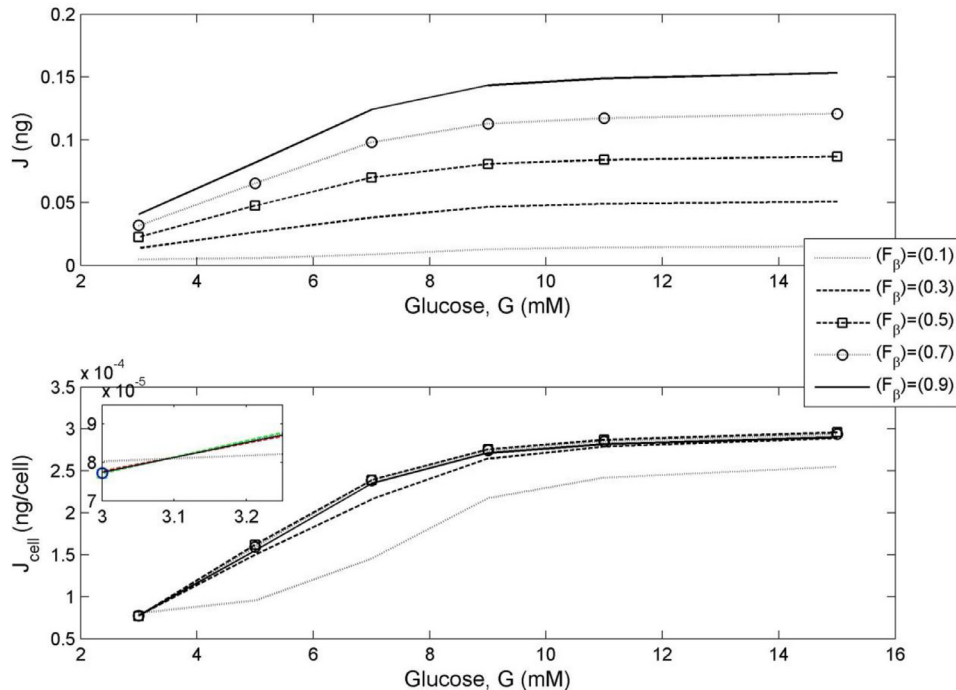


Fig. 6. Total islet insulin secretion increases with glucose dose, and is reduced when there is β -cell loss. Each curve represents mean values averaged from six simulated islets, in response to varying step increases of glucose applied at time $t = 0$ and continued for ten minutes. The top panel shows the total islet insulin secretion while the bottom panel shows the total per cell insulin secretion. Except for the lowest glucose concentration (bottom inset) the total insulin secretion per cell is markedly diminished from islets with the lowest fraction of β -cells ($F_\beta = 0.1$). Parameter values are given in Table A2 column 3, with varying F_β .

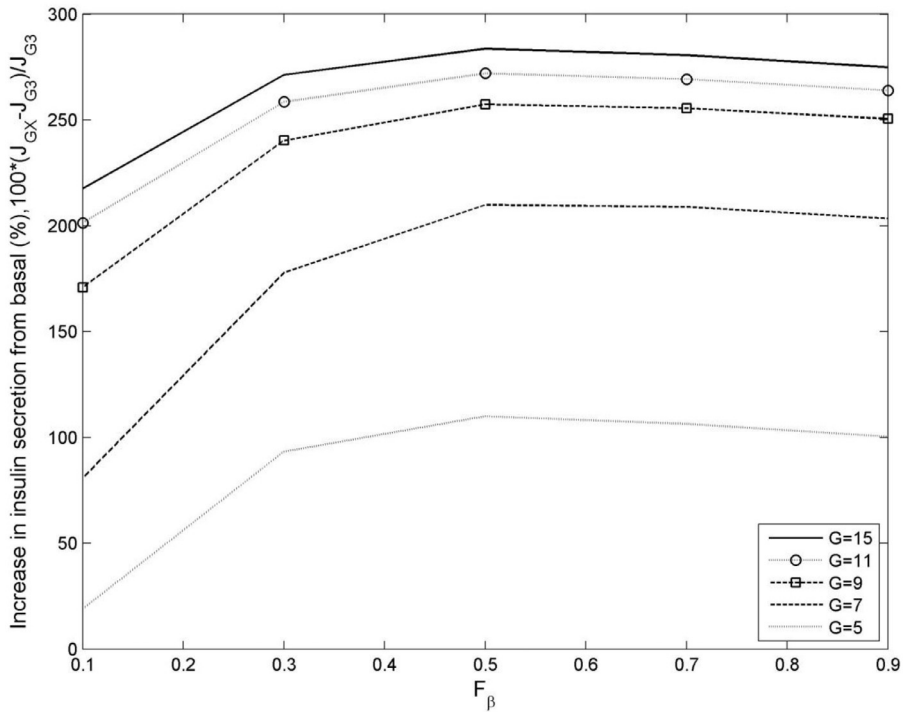


Fig. 7. The glucose dose response of the total islet insulin secretion increases abruptly and plateaus with F_β , the fraction of functional β -cells. Each curve represents mean values averaged from six simulated islets for each value of F_β , in response to varying step increases of glucose applied at time $t=0$ and continued for ten minutes. We show the increase in total islet insulin secretion compared to basal secretion ($G = 3 \text{ mM}$), noting that the increase in secretion is markedly diminished in islets with the lowest fraction of β -cells ($F_\beta = 0.1$). Parameter values are given in Table A2 column 3, with varying F_β .

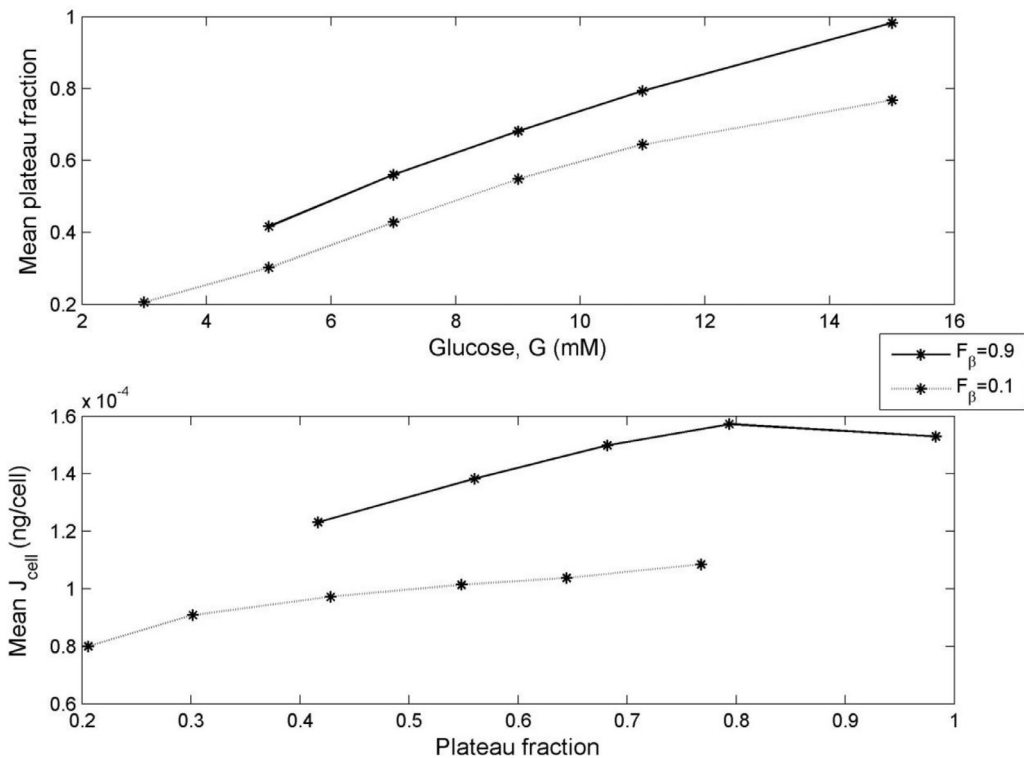


Fig. 8. Glucose affects total insulin secretion through plateau fraction. Plateau fraction increases with higher glucose dose in burster cells (top panel), and the insulin secretion increases generally with larger plateau fraction values, except for the highest glucose dose where cells become spiking (bottom panel). Plateau fractions are higher in islets with a high fraction of β -cells ($F_\beta = 0.9$) than they are in islets with a low fraction of β -cells ($F_\beta = 0.1$). The total insulin secretion increases roughly linearly with increasing plateau fraction. For islets with a high fraction of β -cells, the total insulin secretion decreases between the penultimate and the last data point due to a shift from bursting solutions to spiking solutions. Panels show mean values averaged from six simulations for each F_β . Parameter values are given in Table A2 column 4 with varying F_β .

Previous mathematical models and experimental results (Miura and Pernarowski, 1995; Nunemaker et al., 2006b; Smolen et al., 1993) have indicated that when the glucose concentration is increased the plateau fraction increases, i.e. the active firing phase of the β -cells becomes longer relative to the silent phase. Since Ca^{2+} enters the cell during the active phase through voltage-gated calcium channels and is cleared by Ca^{2+} ATPases during the silent phase, it follows that the glucose dose effect on insulin secretion could be acting through its effect on plateau fraction. Indeed, in Fig. 8 we see that the plateau fraction goes up with increasing glucose concentration (top panel), and that the total insulin secretion is positively correlated with the plateau fraction (bottom panel).

Additionally, Fig. 8 top panel shows that the plateau fraction is higher in islets with a higher β -cell fraction. We note that for such islets the total insulin secretion dips for the last data point (Fig. 8 bottom panel). This is due to a shift from bursting solutions to mainly spiking solutions. At the highest glucose concentration only one out of six islets still features a bursting solution. For the bursting islet the total insulin secretion increases throughout the whole glucose range; for the other five islets the insulin secretion is lower at $G = 15\text{mM}$ than it is at $G = 11\text{mM}$. We remark that in Fig. 8 we used a different parameter set (different values of V_s , θ_s , G_{KATP50} , γ and κ_f compared to Figs. 2–6) for which bursting persists for a wider range of glucose concentrations. For the parameter set used in Figs. 2–6 plots of plateau fraction versus glucose were qualitatively similar (data not shown).

3.3. Potentiation

In Fig. 9 we present results simulating the potentiation experiment (O'Connor et al., 1980; Straub and Sharp, 2002), in which

a step increase in the glucose concentration is followed by a short period at basal glucose before another step increase is applied. Evidently, the experimental observation of a higher second spike in insulin secretion is nicely reproduced (top panel). In the bottom panel, we show the average number of primed granules per cell, $P_{cell}(t) = (\sum_{i=1}^{N_\beta} M_{p,i}(t))/N_\beta$. It shows that the initial spike of the secretory response corresponds to deployment from the primed granule pool. As the primed pool is slowly being refilled over time during the first glucose step, the insulin secretion rises again and becomes biphasic. The larger second secretion spike correlates with the rise in the primed granule pool during the intermittent basal glucose phase, likely explaining the increase over the first peak. Our simulations also revealed that during this phase, refilling of the primed pool occurs from the pool of unprimed granules (data not shown), which has been stimulated by the first period of high glucose. We remark that in simulations of the potentiation experiment using other mathematical models, where the primed and the docked pools were described separately, the higher second “first-phase” secretion was also attributed to the rise in primed granule pool during the low-glucose gap (Chen et al., 2008; Stamper and Wang, 2013). When we varied the islets’ fraction of functional β -cell ($F_\beta = 0.3$ and $F_\beta = 0.1$), we noted that potentiation stayed intact. Simulations with no intracellular coupling ($g_c = 0$) were also qualitatively similar, showing potentiation.

3.4. Ramp followed by multiple glucose steps

Experiments in which a glucose ramp is followed by a period of constant concentration and two step changes (blue dashed lines in Figs. 10 and 11), have been hard to reproduce for many

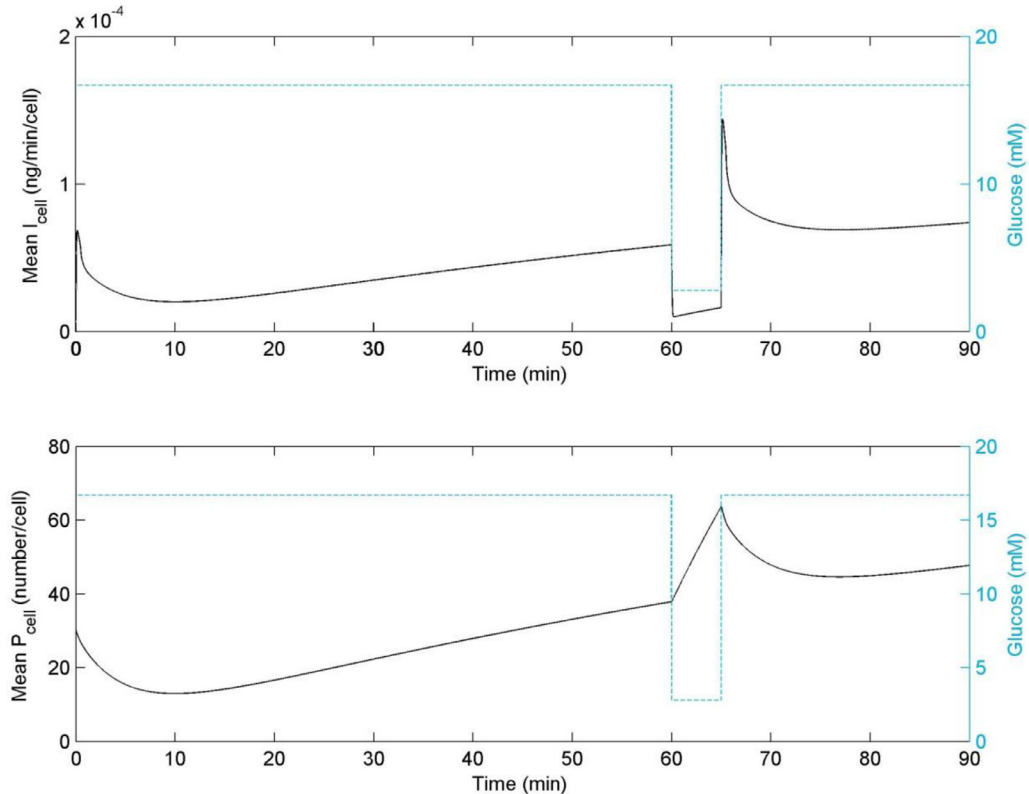


Fig. 9. The new model reproduces the insulin secretion rate pattern observed in potentiation experiments. The second spike in the insulin secretion is higher than the first (top panel). This is due to an increased level of primed granules, P_{cell} , at the time of the second step increase in glucose compared to at the beginning of the experiment (bottom panel). Results presented are mean responses averaged from six simulations obtained from islets of size 57 with 50% functional β -cells, $F_\beta = 0.5$. Parameter values are given in Table A2 column 3.

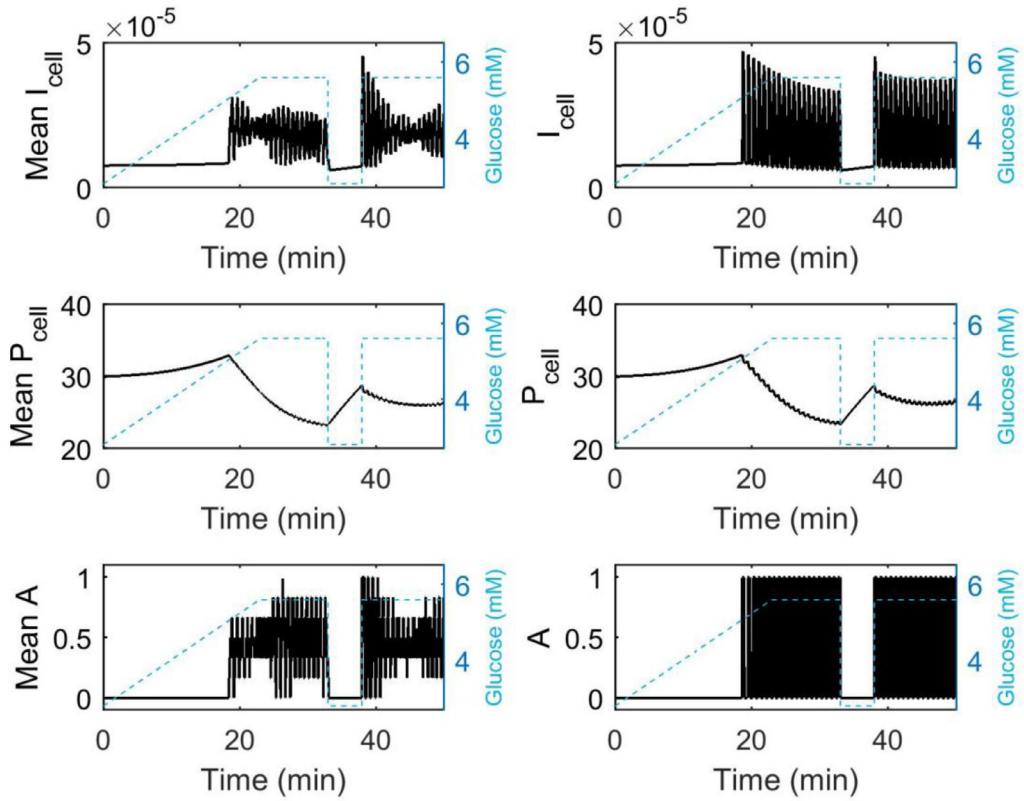


Fig. 10. Simulating observations in the experiment performed on rat pancreata (Fig. 12 in O'Connor et al. (1980)). Left panels show mean responses averaged from six simulations while right panels show responses from one individual example islet. We note that the high insulin spike seen in the averaged response at $t = 38$ min (upper left panel) is due to heterogeneous cell activation between different islets during the initial ramp followed by homogeneous islet activation at the glucose step (bottom left panel, spike is present in the mean activation). Parameter values are given in Table A2 column 3, with $F_\beta = 0.9$.

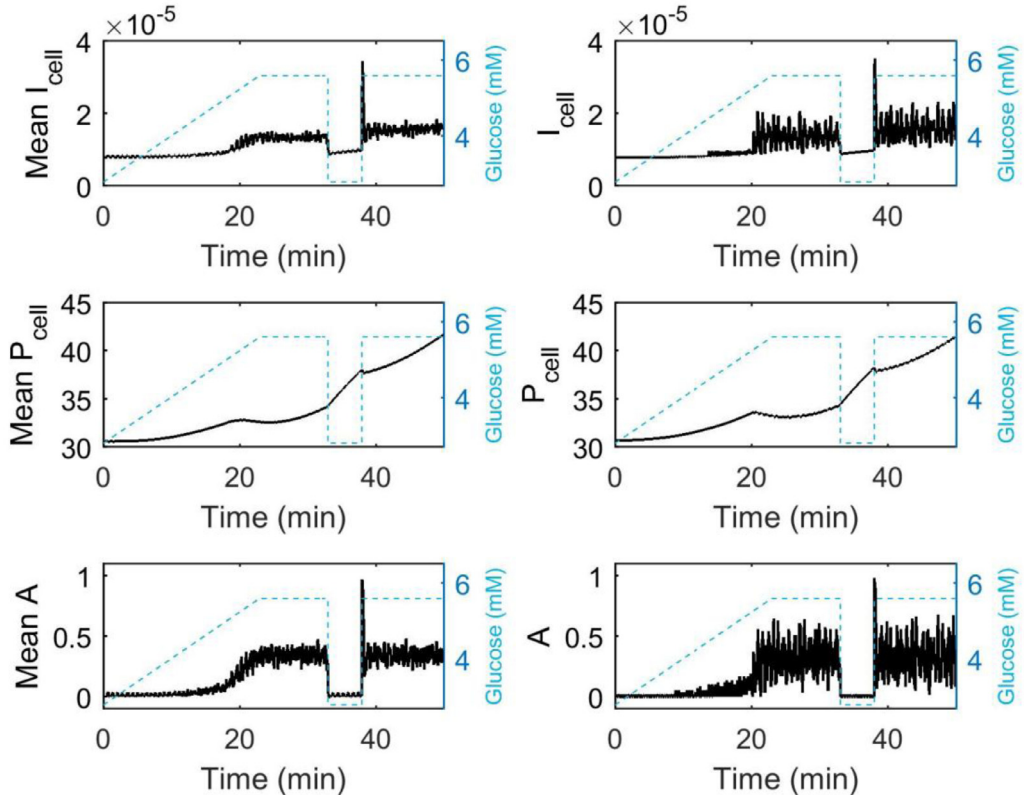


Fig. 11. Simulations representing disintegrated islets subject to the same experimental protocol as in Fig. 10. Panels on the left show mean responses averaged from six simulations while panels on the right show responses from one individual example islet. Both the mean insulin response and the individual islet insulin response display a slow ramp initially followed by a high spike at the last glucose step (at $t = 38$ min). Parameter values are given in Table A2 column 3, with $F_\beta = 0.1$.

mathematical models (O'Connor et al., 1980; Pedersen et al., 2008; Stamper and Wang, 2013). Our integrated mathematical model Fig. 1, Eqs. (1)–(18) is able to replicate the major experimentally observed temporal patterns. In Fig. 10 we present mean results from six intact islets (left panels) and from one example islet (right panels), respectively, responding to such a glucose protocol. We expect the mean (equivalent to sum, noting that pancreata measurements represent the sum from all islets) islet response to reproduce the experimental observations, and indeed, a high spike is evident when the last glucose step is administered (Fig. 10, top left panel), as seen in pancreata experiments (O'Connor et al., 1980; Pedersen et al., 2008). When simulating the potentiation experiment, we found that the elevated second spike relied on an enlarged primed pool at the second glucose step (Fig. 9, bottom panel). In contrast, here, the size of primed granule pool (Fig. 10, middle left panel) cannot explain the higher peak at the last glucose step (Fig. 10, top left panel, at ~38 min). To further investigate the underlying mechanism responsible for the secretion pattern, we examined changes in islet cell activation. We define the islet's instantaneous activity, $A(t)$, ($A(t) \in [0, 1]$), as the fraction of β -cells whose membrane potential satisfies $V(t) > -50$ mV (a similar definition of instantaneous activity, with $V(t) > -53$ mV, was used in Smolen et al. (1993), and present the results in Fig. 10, bottom panels. Evidently, the six different islets activate at slightly different glucose concentrations during the ramp, but they all activate in unison at the beginning of the last glucose step. This suggests that the highest mean insulin secretion rate at the final glucose change may hinge on cell activation in unison. Interestingly the response of individual islets exhibits a different pattern (Fig. 10, top right panel), where cell activation is homogeneous and the insulin secretion rate is more affected by the size of the primed insulin granule pool, resulting in a relatively high spike during the ramp.

In Fig. 11 we present the response for islets with a low fraction of functional β -cells ($F_\beta = 0.1$). Both the mean response (top left panel) and the individual islet response (top right panel) exhibit relatively moderate insulin secretion during the ramp, followed by a high insulin spike at the last glucose step administration. In these highly dysfunctional islets cell activation is heterogeneous during the ramp phase of the experiment, more cells becoming active as the glucose concentration increases. In addition, cell activation occurs virtually in all cells when the last glucose step is applied (at time $t = 38$ min). This activation pattern, together with an increasing size of the primed granule pool, leads to a gradual increase in insulin secretion during the ramp and a high insulin spike at the last glucose step.

3.5. Staircase

Staircase experiments have been performed using both rodent pancreata (O'Connor et al., 1980) and human islets (Dufrane et al., 2007; Henquin et al., 2006). In such experiments, glucose is increased multiple times in a stepwise fashion. We found that in general our mathematical model is able to reproduce the temporal characteristics in insulin secretion. The results for islets subjected to the staircase protocol as used in O'Connor et al. (1980) are shown in Fig. 12, with additional results for small islets of size 57 presented in Appendix D, Fig. A6. In the original experiment (O'Connor et al., 1980), distinct insulin spikes for every glucose step were observed, with the second spike being the largest. Interestingly, for all islets we have simulated, including the disintegrated ones with low $F_\beta=0.1$, distinct insulin secretion peaks after each step increase of glucose are evident (Figs. 12 & A6, top left panels). Additionally, the second step increase elicits the highest amount of insulin secretion. A first look at the per-cell

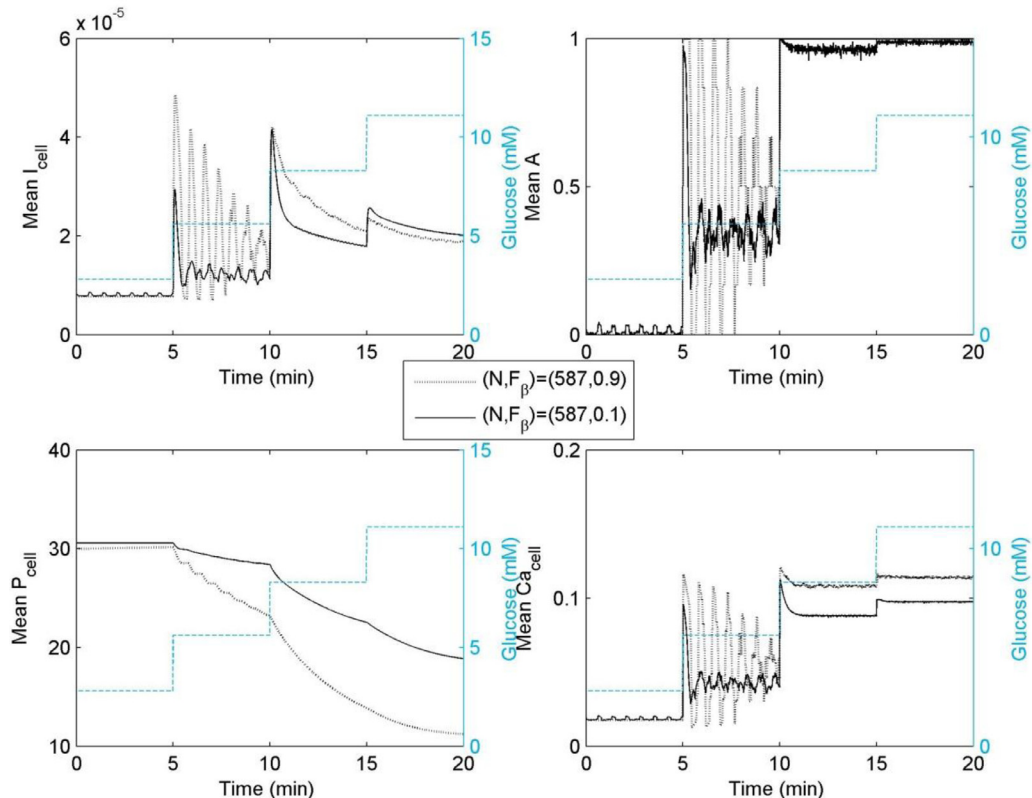


Fig. 12. Simulations of islet staircase experiment. Islets with a low value of F_β display a relatively small first peak in insulin secretion due to relatively low concentrations of intracellular calcium and low activity levels. Panels show mean responses averaged from six simulations. Parameter values are given in Table A2 column 3, with varying F_β and $N = 587$.

insulin secretion rate presented in Fig. 12, top left panel, may lead one to think that the simulated insulin secretion rate from intact islets with $N = 587$, $F_\beta = 0.9$ shows a highest peak after the first step, rather than after the second step as experimentally observed (O'Connor et al., 1980). We remark that in the original rat pancreata staircase experiment (O'Connor et al., 1980) measurements were taken from perfused pancreas rather than single islets; and only 4 time points were sampled during each glucose step, with the first at about 1 min after the start of the glucose step. Thus the study was not able to capture the oscillations in insulin secretion. An appropriate comparison perhaps should examine the total acute insulin secretion (*i.e.* area under curve) during each glucose step rather than the peak. Indeed the model prediction is consistent with experimental results in that the total acute insulin secretion is the highest during the second glucose step.

The other panels of Figs. 12 and A6 may shed light on why the second step elicits the highest acute response. Remember that the insulin secretion rate depends on size of the fused pool (Eq. (18)), and the rate of fusion increases with both the number of primed granules and the intracellular calcium concentration (Eqs. (13) and (17)). Note that the mean calcium concentrations (lower panels) and cell activity levels (top right panels) during the first step are relatively low, thus making relatively low acute secretion. As a consequence, the pools of primed granules stay relatively large (Figs. 12 and A6, lower left panels, the drop in P_{cell} during the first step is the least compared to the subsequent steps). Therefore, the significant increase in glucose and calcium concentrations, combined with the relatively moderate drop in the primed granule pool size, leads to a second spike in insulin secretion that is higher than the first or the third.

4. Discussion

In this paper we have presented and analyzed a new model in which insulin secretion arises from the mobilization, priming and fusion of insulin granules within electrically coupled β -cells arranged in a 3D HCP network. Our new model combines slightly modified versions of two previous models from us: a model for the β -cells' electrical activation, in which membrane potential and intracellular calcium are the main dependent variables (Nittala and Wang, 2008; Nittala et al., 2007); and a model describing insulin secretion via glucose-dependent intracellular granule dynamics (Stamper and Wang, 2013). In order to connect the two we assume that the granule fusion rate is an increasing, saturating function of the intracellular calcium concentration. Furthermore, we accommodate glucose-dependence into the beta cells' electrical response by assuming that the conductance of the K_{ATP} -channel is a decreasing function of glucose. Such a glucose effect is consistent with experimental observations.

We remark here that in this first effort of ours to integrate models of the β -cell's intracellular granule trafficking, its electrophysiology, and its islet cellular network into a multi-scale mathematical model, we took a minimal approach, simplifying or omitting a number of factors. These factors are being considered for future model extensions. For instance, we did not take into account any oscillatory tendency in the conductance that might occur at high glucose due to intrinsic oscillations in the ATP/ADP ratio (Ren et al., 2013). A future version of our model could involve explicitly modeling changes in the ATP/ADP ratio as glucose is altered, as for example has been done in the mathematical models in Bertram et al. (2007) and Pedersen et al. (2005). Based on initial simulations relating to the issue of gap junction coupling heterogeneity (presented in Appendix E), we comment that the major results reported in this paper would likely be robust, if we were to extend our current mathematical model to a more detailed and complex one. Like other biophysical properties of islet

β -cells, the coupling strength between β -cells is known to be heterogeneous. In mouse islets, the values were found to vary from 0 to 600 pS, with distribution mean and standard deviation being 215, and 110 pS, respectively (Perez-Armendariz et al., 1991). In our previous work (Nittala et al., 2007), islets with uniform gap-junctional conductance of varying strength ranging from 25 to 1000 pS were simulated. Others have explicitly incorporated the experimentally observed distribution in their model simulations (Smolen et al., 1993). A recent report suggests that highly heterogeneous gap junctions are important for a mathematical model to reproduce the experimentally observed islet calcium spatiotemporal dynamics (Gosak et al., 2017). However, in our preliminary analysis, we found that incorporating coupling heterogeneity as was done in Smolen et al. (1993) likely would not qualitatively affect the findings reported in this paper (Appendix E, Figs. A7–A8). We note that the question of how heterogeneity in inter- β cell coupling strength impacts the islet electrophysiology is intricately intertwined with other factors such as the heterogeneity in biophysical and biochemical properties of individual β -cells, the number of peers that each β -cell is electrically coupled to, and the structure of the islet's β -cell coupling network. We therefore reserve a thorough investigation of this topic for future studies where we plan to focus more on the relationship between islet structure and function.

Increased basal response is an indicator of islet dysfunction, as for example seen when comparing secretion rates from isolated cells to those of cells aggregated in intact islets (Hopcroft et al., 1985; Speier et al., 2007b). In our simulations we observed that in islets with a high degree of functional β -cells insulin secretion is typically not activated for the lowest glucose step ($G = 3$ mM). In contrast, islets with a low degree of functional β -cells contain subpopulations of active cells, thus secreting more insulin at this glucose dose. We remark that all parameters related to activation (G_m , G_p , C_{af}) are the same throughout the entire β -cell population for all simulations, but yet the islet's structural organization, in this case the extent to which the islet's β -cell network is intact, influences the cells' activation by changing their membrane potential and calcium responses. In particular, in the highly functional islets, the membrane potential and the calcium levels tend to be tightly controlled in all cells, while the less functional islets show more heterogeneity, with a subset of cells activating at the lower glucose level. The cells with the lowest number of nearest neighbors are more likely to become active at basal glucose. Our model analysis shows that as β -cell death progresses more cells have fewer neighbors which allows the cells to respond at low glucose. In addition, we found that the likelihood of cell activation not only depends on an individual cell's number of nearest neighbors, but also on the islet's average number of nearest neighbors (with activation being less likely in islets with higher β -cell fraction). Another study that has looked at islet activation at basal glucose has been presented in Hraha et al. (2014). There, using a Boolean network modeling approach in combination with mutant islets in which a fraction of the cells were made electrically inactive, it was shown that islets experience a phase transition from global activity to inactivity as the number of inexcitable cells becomes greater than a threshold value of roughly 15 percent. An ultimate understanding of islet cell activation may require high-level considerations of the β -cell network topology and connectivity, and of the structure and function relationship in the β -cell network, such as from the perspective of network percolation (Stamper et al., 2014).

For intermediate and high glucose doses, our results show that plateau fraction, calcium levels, cell activation, and the average insulin secretion rate per cell, I_{cell} , increase with glucose concentration, and are generally higher in islets with low degree of β -cell loss than in highly disintegrated islets. These taken together give intact islets a secretory edge. Thus, in islets with a low fraction of

functional β -cells, not only is the insulin secretion diminished due to the fact there are fewer β -cells, but also because the reduced network connectivity has a detrimental effect inherently on each individual β -cell's ability to secrete insulin. Both the number of active cells and the plateau fraction have been shown previously by others to increase with increasing glucose and have been linked to the amount of insulin secreted (Miura and Pernarowski, 1995; Nunemaker et al., 2006b; Smolen et al., 1993). Experimental studies also corroborate the importance of intact islet cell connectivity for a proper glucose dose response. Apart from the improperly increased basal response, cell isolation results in decreased insulin secretion at intermediate, stimulatory glucose concentrations (Hopcroft et al., 1985). Furthermore, in cellular clusters, as opposed to single, isolated cells, activation or recruitment occurs over a narrow range of glucose concentrations, so that secretion can be turned on or off more readily (Heart et al., 2006; Jonkers and Henquin, 2001; Speier et al., 2007a). Our simulation results are consistent with these experimental findings and further indicate the importance of intact cytoarchitecture in islet function.

Along with the model in Notary et al. (2016), ours is one of the few to integrate a granule trafficking model of glucose-induced insulin secretion with a model of islet electrical oscillation within a network of β -cells. The integration allows us to capture the oscillations in the insulin secretion rate that result from oscillatory electrical activity. Our comparison of bursting and spiking cells reveals that bursters may generate more insulin (Fig. 8, bottom panel). This is in line with some previous studies. For example, in Smolen et al. (1993) it was shown that the dose response curve of bursters is steeper than that of spikers. Regarding endocrine pituitary cells, it has also been observed that bursting often leads to more hormone release than spiking does (Tagliavini et al., 2016). From our simulations of glucose steps, we note that as the islet disintegrates due to extensive β -cell loss, the oscillatory nature of the insulin secretory response weakens due to a reduced fraction of burster cells and a loss of synchrony in the electrical response. In addition, oscillations in the insulin secretion are damped as glucose is elevated to a high level. Since impaired oscillations may lead to less effective glucose control (Bratusch-Marrain et al., 1986; Matthews et al., 1983; Satin et al., 2015) and in turn, to higher glucose levels, the fact that both β -cell loss and high glucose affect oscillation negatively could result in a double whammy for the system. Impaired pulsatility is also a hallmark of diabetes (Satin et al., 2015).

Due to the lack of non-invasive imaging technologies, it is currently not possible to establish the exact critical amount of β -cell loss at diagnosis of Type 1 diabetes (Stamper et al., 2014). At present it is estimated that onset occurs when roughly 70–90% of the β -cells have been destroyed (Gepts, 1965; van Belle et al., 2011). We have previously shown that onset may be associated with the loss of percolation within the pancreatic β -cell network (Stamper et al., 2014). Here (in Figs. 5 and 6) we show that there is a clear drop in average insulin secretion per cell for $F_\beta = 0.1$ compared to the other values of F_β that we simulated ($F_\beta \geq 0.3$). Could this drop in average insulin secretion per cell be linked to onset of Type 1 diabetes? The sharp reduction in average insulin secretion per cell would cause cells in the pancreas to experience markedly lower local insulin concentrations, which are likely important for paracrine interactions between pancreatic

cells. For example, insulin secreted by β -cells, or other compounds co-secreted with insulin, may inhibit the release of glucagon by α -cells (Almaca et al., 2016; Cryer, 2012; Ravier and Rutter, 2005). It is interesting to speculate that altered paracrine effects, e.g. abnormal excessive glucagon secretion at high glucose, could play a role in the onset of type 1 diabetes when the fraction of β -cells drops below a certain threshold, thus contributing to hyperglycemia. In the future our model could be extended to include such paracrine interactions which we did not model in this paper.

Our analysis of the glucose ramp experiment shows that the observed spike in insulin secretion relies on homogeneous cell activation. In disintegrated islets with a low fraction of β -cells the insulin secretion increases slowly at the beginning of the experiment as cells gradually become activated when the glucose concentration is being ramped up. Since all cells activate simultaneously at the moment the final glucose step is applied, there is a pronounced spike in the insulin secretion rate at that point. We remark that our simulations suggest that the ramp experiment which features a more prominent second spike in Fig. 11 where the islet's fraction of β -cells is low could potentially be used for clinical detection of β -cell loss.

It has long been appreciated that islet architecture plays an important role in facilitating normal hormone release and paracrine signaling (Arrojo e Drigo et al., 2015; Eberhard and Lammert, 2009). Moreover, it has been shown that islet architectural abnormalities contribute to the development of diabetes (Kilimnik et al., 2011; Morgan et al., 2014). In this paper, our simulations of various glucose protocols reveal the dependence of the insulin secretion rate and its oscillatory nature on the islet parameter F_β , thus displaying the complex relationship between β -cell function (how the islet responds to glucose dose by secreting insulin properly), and β -cell mass (including the structural organization of the mass). This partially explains why the study of this relationship has been challenging. We believe that continued efforts using mathematical modeling to study the islet from the perspective of network theory will lead to new insights into islet function in health and disease.

Acknowledgement

We thank Dr. Arthur Sherman for useful discussions. We also thank an anonymous reviewer for helpful comments and suggestions.

Appendix A. Model variables and parameters

Tables A1 and A2.

Table A1
Model variables.

Variable	Description
V_i	Membrane potential in cell i
$[Ca^{2+}]_i$	Intracellular calcium concentration in cell i
n_i	Activation variable for cell i
s_i	Activation variable for cell i
$M_{u,i}$	Number of unprimed mobilized granules in cell i
$M_{p,i}$	Number of primed mobilized granules in cell i
F_i	Number of fused granules in cell i
t	Time

Table A2**Model parameters.** Values followed by the word mean represent mean values for parameters that vary between individual islet β -cells.

Parameter	Unit	Value in Figs. 2–7, 9–12 and A3–A8	Value Fig. 8	Value Fig. A1–A2	Parameter description
C_m	pF	5300 (mean)	5300 (mean)	5.537×10^3	Membrane capacitance
g_c	pS	200	200	0	Gap-junctional conductance
f	1	0.01	0.01	0.01	Fraction of free Ca^{2+} in the intracellular space
α_i	$\mu\text{M}[\text{fA}]^{-1}[\text{ms}]^{-1}$	4.5×10^{-6} (mean)	4.5×10^{-6} (mean)	4.6133×10^{-6}	Conversion factor for electrical into chemical gradient
$k_{Ca,i}$	$[\text{ms}]^{-1}$	0.6 (mean)	0.2 (mean)	0.2047	Removal rate of Ca^{2+} from the intracellular space
g_{Ca}	pS	1000 (mean)	1000 (mean)	988.29	Maximal conductance of the Ca^{2+} -channel
$g_{K_{ATP}}$	pS	150 (mean)	150 (mean)	158.81	Maximal conductance of the ATP-activated K^+ -channel
g_K	pS	2700 (mean)	2700 (mean)	2.592×10^3	Maximal conductance of the K^+ -channel
g_S	pS	200 (mean)	200 (mean)	183.87	Maximal conductance of the slow-inhibiting K^+ -channel
V_{Ca}	mV	25	25	25	Reversal potential for the Ca^{2+} -channel
V_K	mV	-75	-75	-75	Reversal potential for the K^+ -channel
V_m	mV	-20	-20	-20	Half-maximal potential for the m_∞ curve
θ_m	mV	12	12	12	Voltage constant
V_n	mV	-16	-16	-16	Half-maximal potential for the n_∞ curve
θ_n	mV	5.6	5.6	5.6	Voltage constant
V_s	mV	-52	-57	-57	Half-maximal potential for the s_∞ curve
θ_s	mV	10	5	5	Voltage constant
τ_n	ms	20	20	20	Time constant
τ_s	ms	2×10^4	2×10^4	2×10^4	Time constant
$G_{K_{ATP},50}$	mmol/l	7	10	10	Glucose concentration at which fraction of free K_{ATP} -channels is half-maximal
γ	1	6	2	2	Hill coefficient
m_0	$[\text{ms}]^{-1}$	$1/6 \times 10^{-4}$	$1/6 \times 10^{-4}$	$1/6 \times 10^{-4}$	Basal mobilization rate of unprimed granules
p_{m0}	$[\text{ms}]^{-1}$	$4/6 \times 10^{-7}$	$4/6 \times 10^{-7}$	$4/6 \times 10^{-7}$	Basal rate of priming of unprimed mobilized granules
f_{m0}	$[\text{ms}]^{-1}$	$8/15 \times 10^{-6}$	$8/15 \times 10^{-6}$	$8/15 \times 10^{-6}$	Basal rate of fusion of primed mobilized granules
s	$[\text{ms}]^{-1}$	$1/2 \times 10^{-3}$	$1/2 \times 10^{-3}$	$1/2 \times 10^{-3}$	Rate of insulin secretion
M_{umax}	1	7×10^3	7×10^3	7×10^3	Threshold value of M_u when glucose-induced mobilization of granules toward the plasma membrane ceases
m	$[\text{ms}]^{-1}$	1×10^{-3}	1×10^{-3}	1×10^{-3}	Maximum glucose-induced mobilization rate of unprimed granules
G_m	mmol/l	2.8	2.8	2.8	Glucose concentration at which glucose-induced mobilization of unprimed granules is activated
κ_m	1	1	1	1	Hill coefficient
κ_p	1	1	1	1	Hill coefficient
κ_f	1	1	12	12	Hill coefficient
G_{m50}	mmol/l	14	14	14	Glucose concentration at which mobilization of unprimed granules is half-maximal
p_m	$[\text{ms}]^{-1}$	$1/6 \times 10^{-7}$	$1/6 \times 10^{-7}$	$1/6 \times 10^{-7}$	Maximum glucose-induced priming rate of unprimed mobilized granules
G_p	mmol/l	2.8	2.8	2.8	Glucose concentration at which glucose-induced priming of unprimed granules is activated
G_{p50}	mmol/l	14	14	14	Glucose concentration at which priming of unprimed granules is half-maximal
f_m	$[\text{ms}]^{-1}$	$1.6/6 \times 10^{-4}$	$1.6/6 \times 10^{-4}$	$1.6/6 \times 10^{-4}$	Maximum calcium-induced fusion rate of primed mobilized granules
Ca_f	$\mu\text{mol/l}$	0.07	0.07	0.07	Intracellular calcium concentration at which calcium-induced fusion of primed granules is activated
Ca_{f50}	$\mu\text{mol/l}$	0.4	0.4	0.4	Intracellular calcium concentration at which fusion of primed granules is half-maximal
I_g	ng	8×10^{-6}	8×10^{-6}	8×10^{-6}	Insulin content of one granule
N	1	587	587	N/A	Number of cells per islet

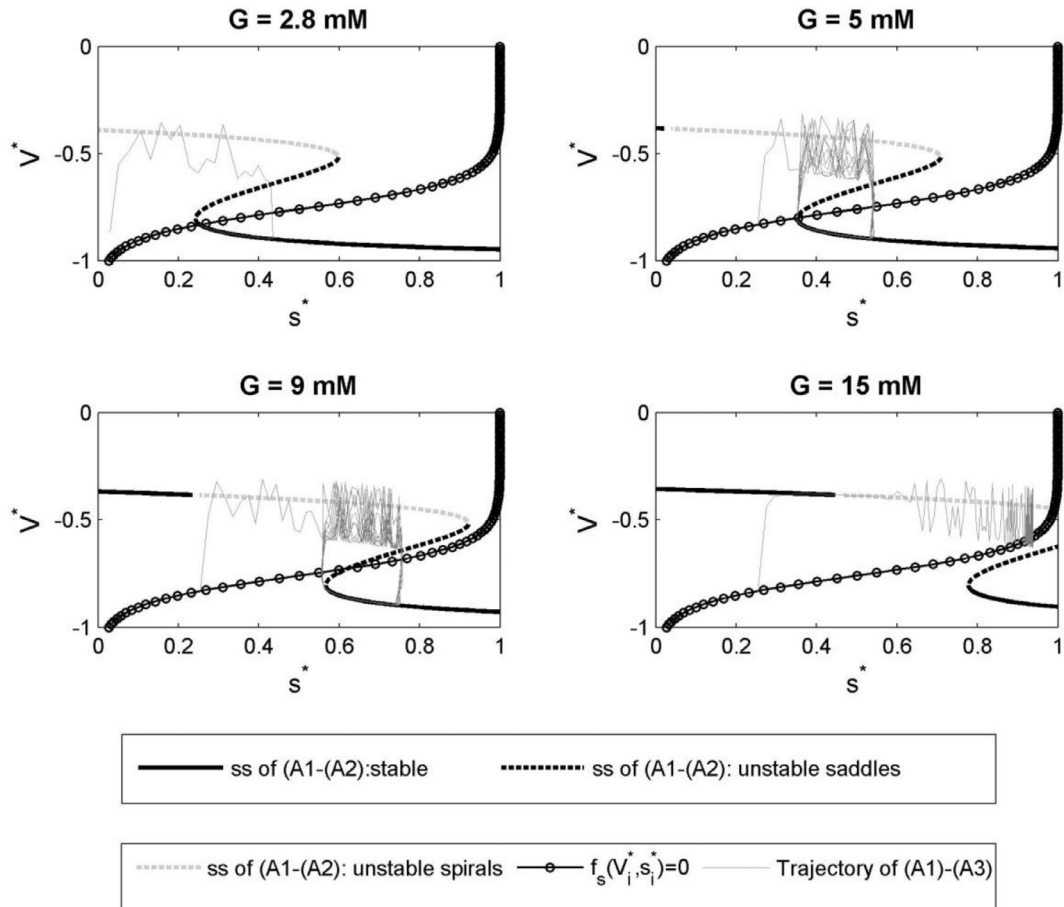


Fig. A1. Bifurcation diagram of single, unconnected β -cells showing how the steady states of the membrane potential in the fast subsystem depend on the slow variable s_i^* . Four panels corresponding to four different glucose concentrations. For the lowest glucose concentration the solution evolves to a linearly stable steady state (the intersection of the nullclines). At intermediate glucose concentrations a bursting solution is observed. At high glucose the solution corresponds to constant firing. Parameter values are listed in Table A2, column 5.

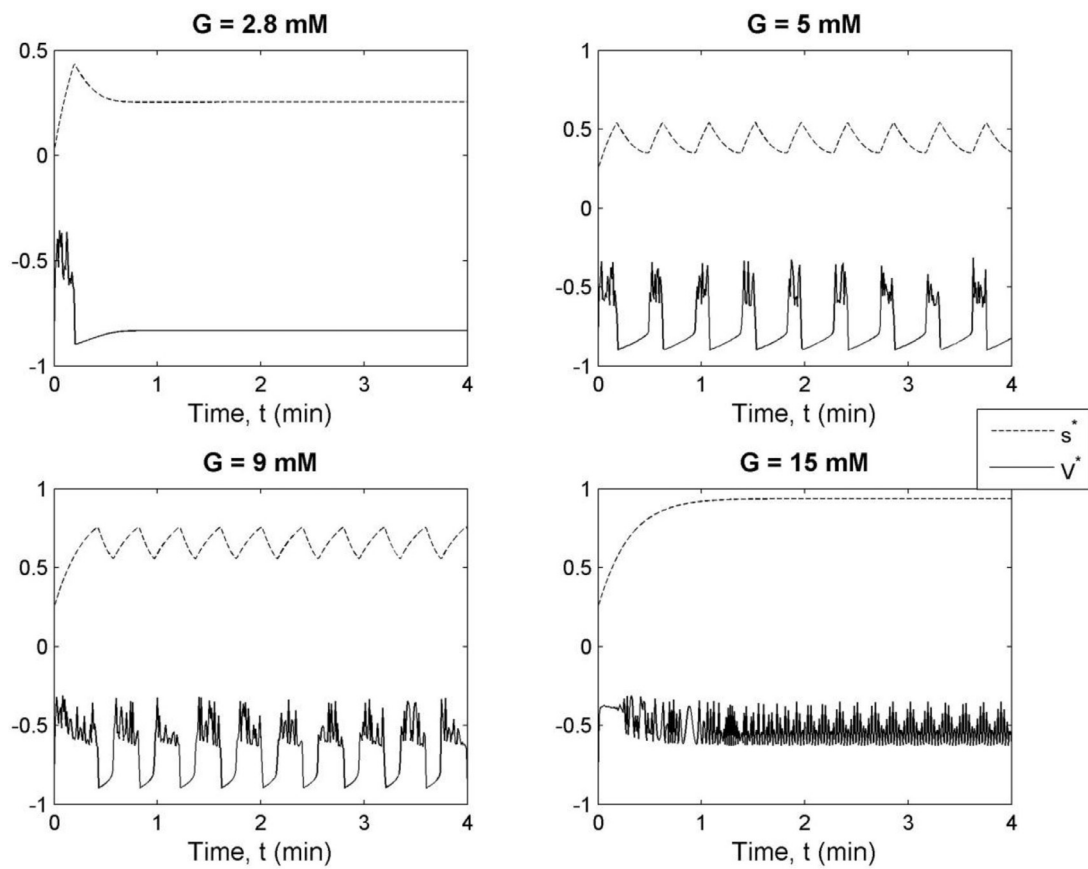


Fig. A2. The evolutions of s^* and V^* in time at four different glucose concentrations. For the lowest glucose concentration, the solution evolves to a linearly stable steady state. At intermediate glucose concentrations a bursting solution is observed featuring intervals of oscillations rapidly interrupted by intervals of electrical silence. At high glucose the solution corresponds to constant firing. Parameter values are same as in Fig. A1, and are listed in Table A2, column 5.

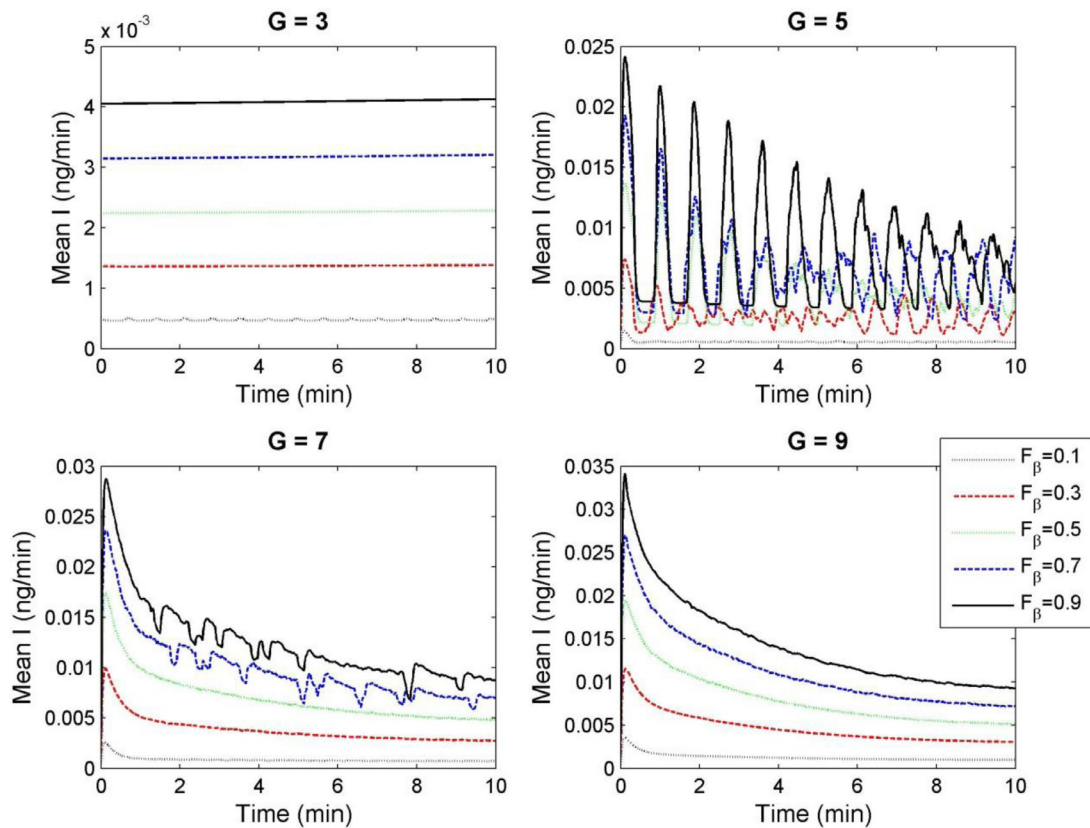


Fig. A3. Insulin secretion rates from islets of different composition in response to four different step increases of the glucose concentration. Each response was calculated as the mean from six islets with the same F_β . With the exception of the lowest glucose case, oscillations in the insulin secretion rate are dampened both by β -cell loss and by high glucose. At $G = 7$ mM only a subset of the islets with $F_\beta \geq 0.7$ features bursting solutions. Parameter values as in Fig. 2.

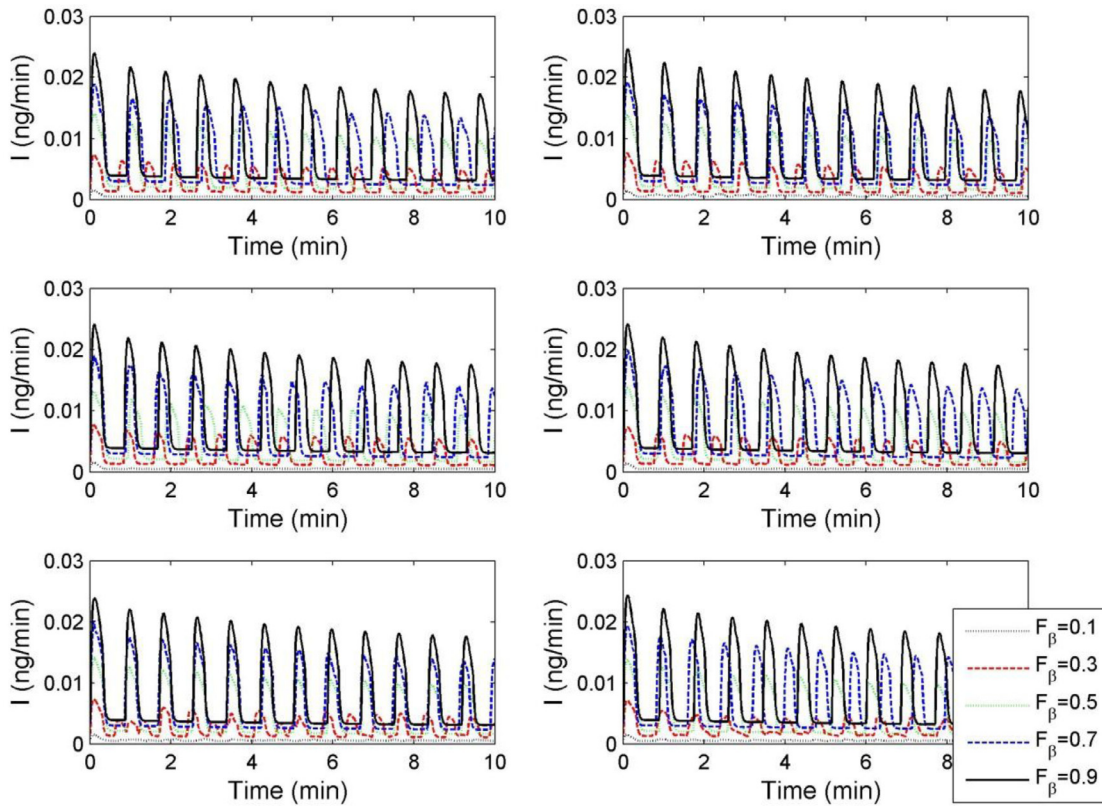


Fig. A4. Insulin secretion rates from islets of different composition in response to a step increase of the glucose concentration from basal to $G = 5$ mM. Each panel shows the responses of five islets with varying F_β . All five islets within each panel were initiated with the same random seed; a different random seed was used for each of the six panels. At this glucose concentration insulin secretion is oscillatory for $F_\beta \geq 0.3$ due to bursting. Islets with $F_\beta = 0.1$ feature suppressed oscillations due to a mix of bursting, spiking and silent cells. Parameter values as in Fig. 2.

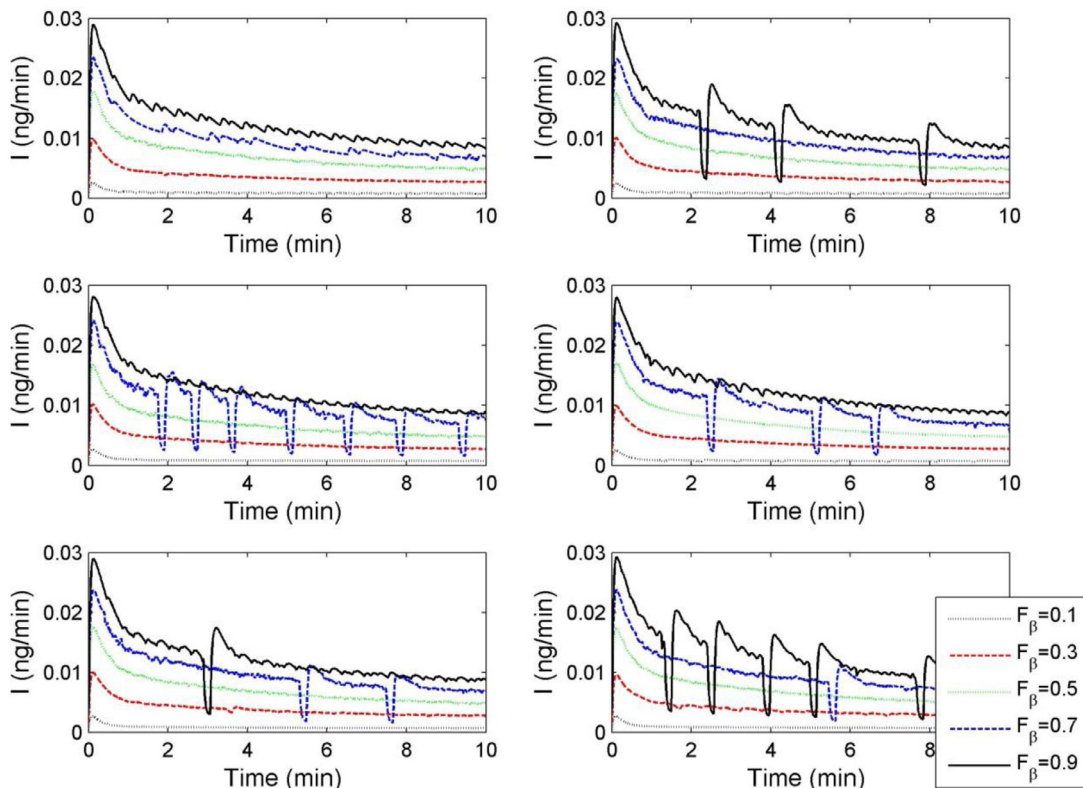


Fig. A5. Insulin secretion rates from islets of different composition in response to a step increase of the glucose concentration from basal to $G = 7$ mM. Each panel shows the responses of five islets with varying F_β . All five islets within each panel were initiated with the same random seed; different random seeds were used for all six panels. At this glucose concentration, only a subset of the islets with either $F_\beta = 0.9$ or $F_\beta = 0.7$ features pronounced oscillations due to bursting. The majority of the islets contain only spiking cells and shows suppressed oscillations. Parameter values as in Fig. 2.

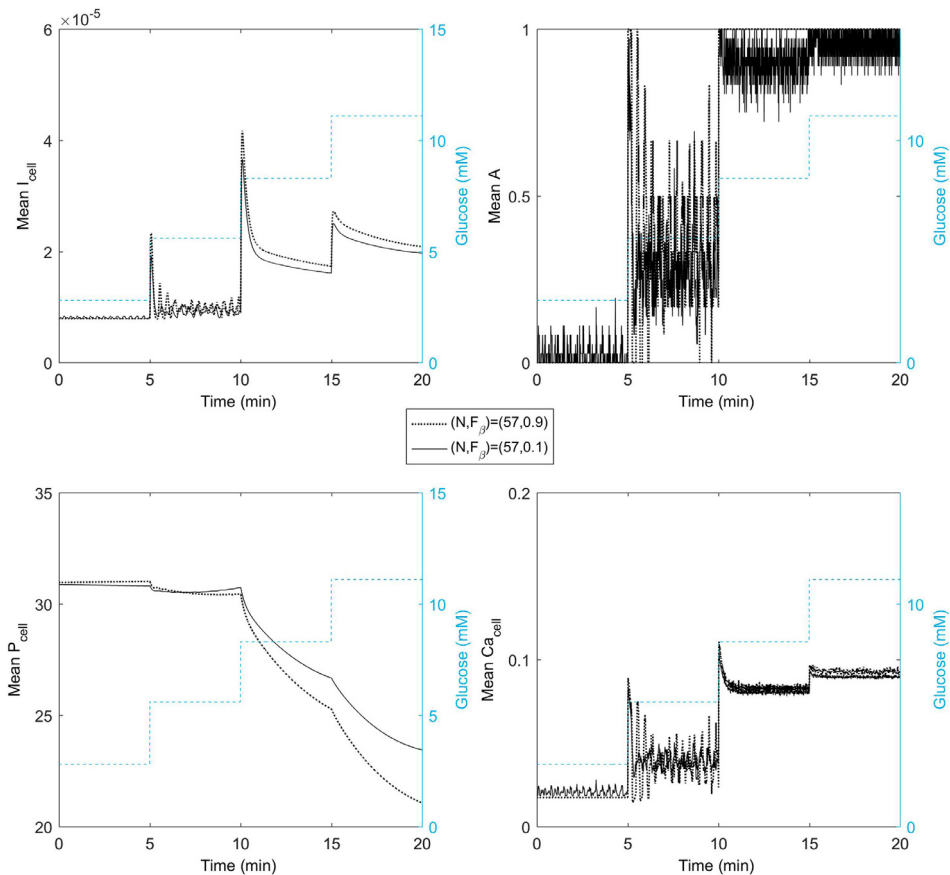


Fig. A6. Simulations of islet staircase experiment. Irrespective of F_β , small islets ($N = 57$) display a staircase pattern with a relatively small first peak in insulin secretion due to relatively low concentrations of intracellular calcium and low activity levels. Panels show mean responses averaged from six simulations. Parameter values are given in Table A2 column 3, with varying F_β and $N = 57$.

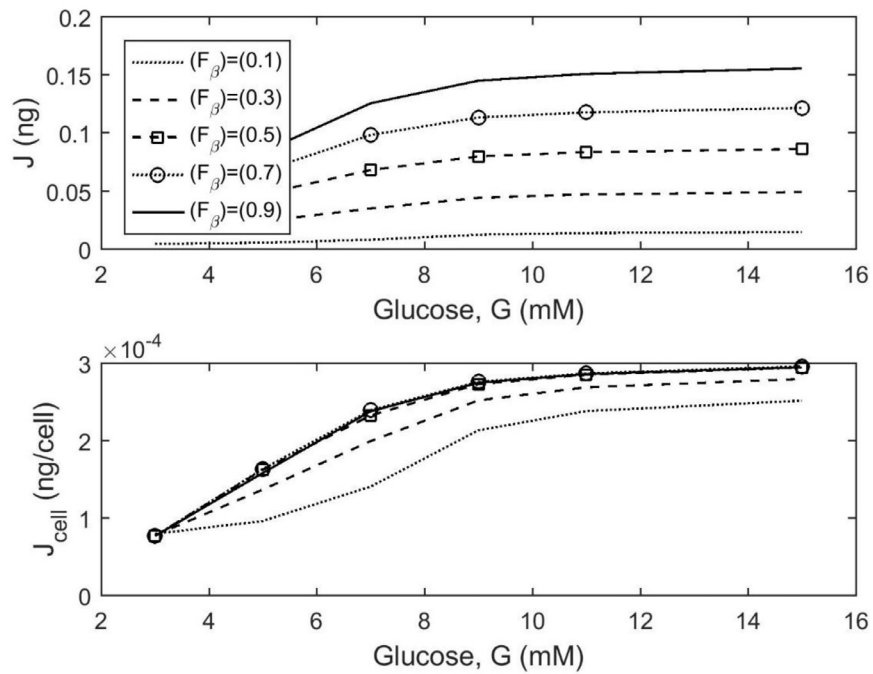


Fig. A7. Total islet insulin secretion increases with glucose dose, and is reduced when there is β -cell loss. Simulation for islets with the same model parameters configurations as those in Fig. 6, except for the gap junction coupling strength g_c , which was sampled from a distribution reported in Perez-Armendariz et al. (1991).

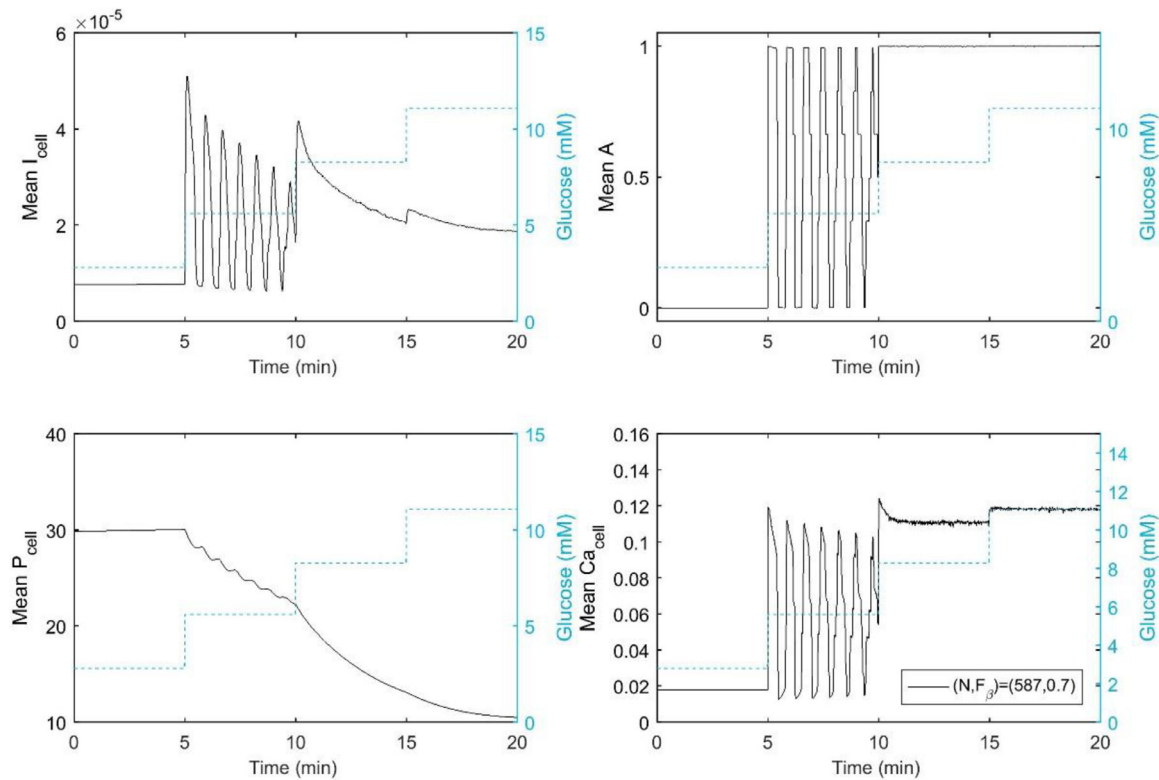


Fig. A8. Simulations of islets with heterogeneous gap junction coupling strength subject to the staircase glucose stimulation protocol. Parameter values are given in Table A2 column 3, with $N = 587$ and $F_\beta = 0.7$, with g_c sampled from a distribution reported in Perez-Armendariz et al. (1991).

Appendix B. Analysis of the membrane potential of single, unconnected β -cells

In order to gain insight into the evolution of the membrane potential for single unconnected β -cells, the model Eqs. (1) and (7)–(8) can be analyzed as a subsystem with $g_c^* = 0$. The equations can be nondimensionalized by scaling each of the variables by its characteristic value. We introduce the following dimensionless variables:

$$t^* = \frac{t}{\tau_n}, \quad V_i^* = -\frac{V_i}{V_K}, \quad n_i^* = n_i, \quad s_i^* = s_i$$

With the above rescalings and with $g_c^* = 0$ the equations transform as:

$$\begin{aligned} \frac{dV_i^*}{dt^*} &= - \left[\frac{\frac{g_{Ca,i}^*(V_i^* - V_{Ca}^*)}{1 + \exp(\frac{V_m^* - V_i^*}{\theta_m})} + \frac{g_{K_{ATP},i}^*(V_i^* - V_K^*)}{1 + \left(\frac{G}{G_{K_{ATP}50}}\right)^{\gamma}}}{1 + \exp(\frac{V_m^* - V_i^*}{\theta_m})} \right. \\ &\quad \left. + g_{K,i}^* n_i^* (V_i^* - V_K^*) + g_{s,i}^* s_i^* (V_i^* - V_K^*) \right] \\ &\stackrel{\text{def}}{=} f_V(V_i^*, n_i^*), \end{aligned} \quad (\text{A1})$$

$$\frac{dn_i^*}{dt^*} = \frac{1}{1 + \exp((V_n^* - V_i^*)/\theta_n)} - n_i^* \stackrel{\text{def}}{=} f_n(V_i^*, n_i^*), \quad (\text{A2})$$

$$\frac{ds_i^*}{dt^*} = \varepsilon \left[\frac{1}{1 + \exp((V_s^* - V_i^*)/\theta_s)} - s_i^* \right] \stackrel{\text{def}}{=} f_s(V_i^*, s_i^*), \quad (\text{A3})$$

with the following groups of dimensionless parameters:

$$\begin{aligned} \varepsilon &= \frac{\tau_n}{\tau_s}, \quad g_{c,i}^* = \frac{g_c \tau_n}{C_{m,i}}, \quad g_{Ca,i}^* = \frac{g_{Ca,i} \tau_n}{C_{m,i}}, \quad g_{K,i}^* = \frac{g_{K,i} \tau_n}{C_{m,i}}, \\ g_{K_{ATP},i}^* &= \frac{g_{K_{ATP},i} \tau_n}{C_{m,i}}, \quad g_{s,i}^* = \frac{g_{s,i} \tau_n}{C_{m,i}}, \quad V_{Ca}^* = -\frac{V_{Ca}}{V_K}, \quad V_K^* = -\frac{V_K}{V_K}, \\ V_m^* &= -\frac{V_m}{V_K}, \quad V_n^* = -\frac{V_n}{V_K}, \quad V_s^* = -\frac{V_s}{V_K}, \quad \theta_m^* = -\frac{\theta_m}{V_K}, \\ \theta_n^* &= -\frac{\theta_n}{V_K}, \quad \theta_s^* = -\frac{\theta_s}{V_K} \end{aligned}$$

We note that $\varepsilon \ll 1$ (for our parameter values $\varepsilon = 0.001$). The fast subsystem is the $O(1)$ system (A1)–(A2) in which s_i^* is treated like a constant parameter (we refer the reader to (Murray, 2002) for more on this type of analysis). In Fig. A1 we show how the steady states of the (nondimensionalized) membrane potential in the fast subsystem depend on the slow variable s_i^* for four different glucose concentrations. In each subplot, the steady states are given by the z-shaped curve which is the null cline $f_V(V_i^*, n_i^*) = 0$, with n_i^* assumed to be at steady state, i.e. obtained by setting the null cline $f_n(V_i^*, n_i^*) = 0$ and solving for n_i^* . We note that there exists a region where three steady states are possible. The steady states on the lower branch are linearly stable (since $\text{tr } A < 0 < \det A$, where A is the 2×2 Jacobian matrix of the fast subsystem (A1)–(A2)), while the steady states in the middle are saddles (since $\det A < 0$) and thus unstable. On the left portion of the upper branch (not visible in top left panel) the steady states are linearly stable. The steady states on the upper branch become linearly unstable (spirals) via a Hopf bifurcation as s_i^* crosses a critical value. As s_i^* slowly varies, the solutions to the system (A1)–(A3) has the potential to jump between the different branches of the z-curve. The solutions that may result from the slow variation in s_i^* are typical of relaxation oscillators, which exhibit rapidly varying intervals interrupted by slowly varying ones (Murray, 2002). The exact nature of the resulting solutions depends on where the z-curve

intersects the nullcline $f_s(V_i^*, s_i^*) = 0$ (note also that the z-curve is shifted to the right as the glucose concentration, G , increases). In Fig. A1, if the intersection occurs where the steady states of the fast subsystem are linearly stable, the system will evolve to a stable steady state (top left panel in Fig. A1). If the intersection is on the unstable part of the upper branch of the z-curve (bottom right panel in Fig. A1), then the membrane potential of the system evolves to sustained oscillations. For intersections in the middle part, where the steady states are unstable saddles, the membrane potential features bursting, jumping rapidly between an oscillatory limit cycle solution (the active burst phase) and a stable steady state (the inactive, silent phase). In Fig. A2 we plot the membrane potential and s_i^* versus time for the four different cases shown in Fig. A1.

Appendix C. Additional figures related to Section 3.2

In Fig. A3 we present the mean insulin secretion rate for islets of different F_β . Figs. A4 and A5 show the individual islet responses to a glucose step of $G = 5 \text{ mM}$, and $G = 7 \text{ mM}$, respectively. Two islets with the same degree of β -cell loss, but initiated with different random seeds, can respond differently to the same glucose protocol due to varying islet composition (the functional β -cells being located at different sites). In general, the islets may be bursting or spiking islets, i.e. only featuring bursting or spiking cells, or mixed islets, consisting of bursting and spiking cells and/or inactive cells.

Appendix D. Additional figures related to Section 3.5

In Fig. A6 we present the mean insulin secretion rates from small islets of size 57 and different F_β during a glucose staircase. The insulin secretion profiles are similar irrespective of F_β , displaying a small first peak due to relatively small calcium and activity levels during the first glucose step.

Appendix E. Additional figures showing simulations with heterogeneous gap-junctional coupling (see related comments in Discussion section)

Our integrated multiscale model (Fig. 1, Sections 2.1–2.2, and results presented in Section 3) did not take into account the reported heterogeneity in gap-junctional coupling strength, g_c , between β -cells (Perez-Armendariz et al., 1991). Here we present a preliminary analysis of an extended model version where the heterogeneity in g_c values is considered. Our results in Figs. A7 and A8 suggest that there is likely no qualitative difference from the major findings reported in Section 3 of this paper. In accordance with the modeling described in (Smolen et al., 1993), in Figs. A7 and A8 we randomly assigned g_c according to the experimental distribution reported in (Perez-Armendariz et al., 1991). In particular, 33 percent of pairs have zero conductance, while the remaining pairs vary in conductance from 25 pS up to 600 pS (mean $215 \pm 110 \text{ pS}$).

References

- Ahren, J., Ahren, B., Wierup, N., 2010. Increased beta-cell volume in mice fed a high-fat diet: a dynamic study over 12 months. *Islets* 2, 353–356. doi: [10.4161/islets.2.6.13619](https://doi.org/10.4161/islets.2.6.13619).
- Almaca, J., Molina, J., Menegaz, D., Promin, A.N., Tamayo, A., Slepak, V., Berggren, P.O., Caicedo, A., 2016. Human beta cells produce and release serotonin to inhibit glucagon secretion from alpha cells. *Cell Rep.* 17, 3281–3292. doi: [10.1016/j.celrep.2016.11.072](https://doi.org/10.1016/j.celrep.2016.11.072).
- Arrojo e Drigo, R., Ali, Y., Diez, J., Srinivasan, D.K., Berggren, P.O., Boehm, B.O., 2015. New insights into the architecture of the islet of Langerhans: a focused cross-species assessment. *Diabetologia* 58, 2218–2228. doi: [10.1007/s00125-015-3699-0](https://doi.org/10.1007/s00125-015-3699-0).
- Ashcroft, F.M., Rorsman, P., 1989. Electrophysiology of the pancreatic beta-cell. *Prog. Biophys. Mol. Biol.* 54, 87–143.

- Barg, S., Huang, P., Eliasson, L., Nelson, D.J., Obermuller, S., Rorsman, P., Thevenod, F., Renstrom, E., 2001. Priming of insulin granules for exocytosis by granular Cl⁻ uptake and acidification. *J. Cell Sci.* 114, 2145–2154.
- Benninger, R.K., Head, W.S., Zhang, M., Satin, L.S., Piston, D.W., 2011. Gap junctions and other mechanisms of cell-cell communication regulate basal insulin secretion in the pancreatic islet. *J. Physiol.* 589, 5453–5466. doi:10.1113/jphysiol.2011.218909.
- Bergsten, P., Hellman, B., 1993. Glucose-induced amplitude regulation of pulsatile insulin secretion from individual pancreatic islets. *Diabetes* 42, 670–674.
- Bertram, R., Satin, L.S., Pedersen, M.G., Luciani, D.S., Sherman, A., 2007. Interaction of glycolysis and mitochondrial respiration in metabolic oscillations of pancreatic islets. *Biophys. J.* 92, 1544–1555. doi:10.1529/biophysj.106.097154.
- Bertuzzi, A., Salinari, S., Mingrone, G., 2007. Insulin granule trafficking in beta-cells: mathematical model of glucose-induced insulin secretion. *Am. J. Physiol. Endocrinol. Metab.* 293, E396–E409.
- Bratusch-Marrain, P.R., Komjati, M., Waldhausl, W.K., 1986. Efficacy of pulsatile versus continuous insulin administration on hepatic glucose production and glucose utilization in type I diabetic humans. *Diabetes* 35, 922–926.
- Cabrera, O., Berman, D.M., Kenyon, N.S., Ricordi, C., Berggren, P.-O., Alejandro Caicedo, A., 2006. The unique cytoarchitecture of human pancreatic islets has implications for islet cell function. *Proc. Natl. Acad. Sci. U.S.A.* 103, 2334–2339.
- Chay, T.R., Keizer, J., 1983. Minimal model for membrane oscillations in the pancreatic beta-cell. *Biophys. J.* 42, 181–190.
- Chen, Y.D., Wang, S., Sherman, A., 2008. Identifying the targets of the amplifying pathway for insulin secretion in pancreatic beta-cells by kinetic modeling of granule exocytosis. *Biophys. J.* 95, 2226–2241. doi:10.1529/biophysj.107.124990.
- Cryer, P.E., 2012. Minireview: glucagon in the pathogenesis of hypoglycemia and hyperglycemia in diabetes. *Endocrinology* 153, 1039–1048. doi:10.1210/en.2011-1499.
- Curry, D.L., Bennett, L.L., Grodsky, G.M., 1968. Dynamics of insulin secretion by the perfused rat pancreas. *Endocrinology* 83, 572–584.
- Dishinger, J.F., Reid, K.R., Kennedy, R.T., 2009. Quantitative monitoring of insulin secretion from single islets of Langerhans in parallel on a microfluidic chip. *Anal. Chem.* 81, 3119–3127. doi:10.1021/ac900109t.
- Dufrane, D., Nenquin, M., Henquin, J.C., 2007. Nutrient control of insulin secretion in perfused adult pig islets. *Diabetes Metab.* 33, 430–438. doi:10.1016/j.diabet.2007.05.001.
- Eberhard, D., Lammert, E., 2009. The pancreatic beta-cell in the islet and organ community. *Curr. Opin. Genet. Dev.* 19, 469–475. doi:10.1016/j.gde.2009.07.003.
- Fujimoto, S., Tsuura, Y., Ishida, H., Tsuji, K., Mukai, E., Kajikawa, M., Hamamoto, Y., Takeda, T., Yamada, Y., Seino, Y., 2000. Augmentation of basal insulin release from rat islets by preexposure to a high concentration of glucose. *Am. J. Physiol. Endocrinol. Metab.* 279, E927–E940.
- Gepts, W., 1965. Pathologic anatomy of the pancreas in juvenile diabetes mellitus. *Diabetes* 14, 619–633.
- Gosak, M., Stozer, A., Markovic, R., Dolensek, J., Perc, M., Rupnik, M.S., Marhl, M., 2017. Critical and supercritical spatiotemporal calcium dynamics in beta cells. *Front. Physiol.* 8, 1106. doi:10.3389/fphys.2017.01106.
- Grodsky, G.M., 1972. A threshold distribution hypothesis for packet storage of insulin and its mathematical modeling. *J. Clin. Invest.* 51, 2047–2059. doi:10.1172/JC107011.
- Head, W.S., Orseth, M.L., Nunemaker, C.S., Satin, L.S., Piston, D.W., Benninger, R.K., 2012. Connexin-36 gap junctions regulate in vivo first- and second-phase insulin secretion dynamics and glucose tolerance in the conscious mouse. *Diabetes* doi:10.2337/db11-1312.
- Heart, E., Corkey, R.F., Wikstrom, J.D., Shirihai, O.S., Corkey, B.E., 2006. Glucose-dependent increase in mitochondrial membrane potential, but not cytoplasmic calcium, correlates with insulin secretion in single islet cells. *Am. J. Physiol. Endocrinol. Metab.* 290, E143–E148.
- Henquin, J.C., Dufrane, D., Nenquin, M., 2006. Nutrient control of insulin secretion in isolated normal human islets. *Diabetes* 55, 3470–3477.
- Hopcroft, D.W., Mason, D.R., Scott, R.S., 1985. Structure-function relationships in pancreatic islets: support for intraislet modulation of insulin secretion. *Endocrinology* 117, 2073–2080. doi:10.1210/endo-117-5-2073.
- Hraha, T.H., Westacott, M.J., Pozzoli, M., Notary, A.M., McClatchey, P.M., Benninger, R.K., 2014. Phase transitions in the multi-cellular regulatory behavior of pancreatic islet excitability. *PLoS Comput. Biol.* 10, e1003819. doi:10.1371/journal.pcbi.1003819.
- Jonkers, F.C., Henquin, J.C., 2001. Measurements of cytoplasmic Ca²⁺ in islet cell clusters show that glucose rapidly recruits beta-cells and gradually increases the individual cell response. *Diabetes* 50, 540–550.
- Kanno, T., Rorsman, P., Gopel, S.O., 2002. Glucose-dependent regulation of rhythmic action potential firing in pancreatic beta-cells by K(ATP)-channel modulation. *J. Physiol.* 545, 501–507. doi:PHY_031344.
- Kilimnik, G., Zhao, B., Jo, J., Periwal, V., Witkowski, P., Misawa, R., Hara, M., 2011. Altered islet composition and disproportionate loss of large islets in patients with type 2 diabetes. *PLoS One* 6, e27445. doi:10.1371/journal.pone.0027445.
- MacDonald, P.E., Joseph, J.W., Rorsman, P., 2005. Glucose-sensing mechanisms in pancreatic beta-cells. *Philos. Trans. R. Soc. Lond. B Biol. Sci.* 360, 2211–2225.
- Marinelli, I., Vo, T., Gerardo-Giorda, L., Bertram, R., 2018. Transitions between bursting modes in the integrated oscillator model for pancreatic beta-cells. *J. Theor. Biol.* 454, 310–319. doi:10.1016/j.jtbi.2018.06.017.
- Matthews, D.R., Naylor, B.A., Jones, R.G., Ward, G.M., Turner, R.C., 1983. Pulsatile insulin has greater hypoglycemic effect than continuous delivery. *Diabetes* 32, 617–621.
- McKenna, J.P., Dhumpa, R., Mukhitov, N., Roper, M.G., Bertram, R., 2016a. Glucose oscillations can activate an endogenous oscillator in pancreatic islets. *PLoS Comput. Biol.* 12, e1005143. doi:10.1371/journal.pcbi.1005143.
- McKenna, J.P., Ha, J., Merrins, M.J., Satin, L.S., Sherman, A., Bertram, R., 2016b. Ca²⁺ effects on ATP production and consumption have regulatory roles on oscillatory islet activity. *Biophys. J.* 110, 733–742. doi:10.1016/j.bpj.2015.11.3526.
- Meda, P., 2012. The in vivo beta-to-beta-cell chat room: connexin connections matter. *Diabetes* 61, 1656–1658.
- Miura, R.M., Pernarowski, M., 1995. Correlations of rates of insulin release from islets and plateau fractions for beta-cells. *Bull. Math. Biol.* 57, 229–246. doi:10.1016/0092-8240(94)00035-B.
- Morgan, N.G., Leete, P., Foulis, A.K., Richardson, S.J., 2014. Islet inflammation in human type 1 diabetes mellitus. *IUBMB Life* 66, 723–734. doi:10.1002/iub.1330.
- Murray, J.D., 2002. Mathematical biology: I. An introduction. Springer, New York.
- Nagamatsu, S., Ohara-Imaizumi, M., Nakamichi, Y., Kikuta, T., Nishiwaki, C., 2006. Imaging docking and fusion of insulin granules induced by antidiabetes agents: sulfonylurea and glinide drugs preferentially mediate the fusion of newcomer, but not previously docked, insulin granules. *Diabetes* 55, 2819–2825. doi:10.2337/db06-0105.
- Nittala, A., Wang, X., 2008. The hyperbolic effect of density and strength of inter-cell coupling in islet bursting. *Theor. Biol. Med. Model.* 5 doi:10.1186/1742-4682-5-17.
- Nittala, A., Ghosh, S., Wang, X., 2007. Investigating the role of islet cytoarchitecture in its oscillation using a new beta-cell cluster model. *PLoS ONE* 2, e983.
- Notary, A.M., Westacott, M.J., Hraha, T.H., Pozzoli, M., Benninger, R.K., 2016. Decreases in gap junction coupling recovers Ca²⁺- and insulin secretion in neonatal diabetes mellitus. Dependent on Beta Cell Heterogeneity and Noise. *PLoS Comput. Biol.* 12, e1005116. doi:10.1371/journal.pcbi.1005116.
- Nunemaker, C.S., Wasserman, D.H., McGuinness, O.P., Sweet, I.R., Teague, J.C., Satin, L.S., 2006a. Insulin secretion in the conscious mouse is biphasic and pulsatile. *Am. J. Physiol. Endocrinol. Metab.* 290, E523–E529.
- Nunemaker, C.S., Bertram, R., Sherman, A., Tsanava-Atanasova, K., Daniel, C.R., Satin, L.S., 2006b. Glucose modulates [Ca²⁺]i oscillations in pancreatic islets via ionic and glycolytic mechanisms. *Biophys. J.* 91, 2082–2096.
- O'Connor, M.D., Landahl, H., Grodsky, G.M., 1980. Comparison of storage- and signal-limited models of pancreatic insulin secretion. *Am. J. Physiol.* 238, R378–R389.
- O'Rahilly, S., Turner, R.C., Matthews, D.R., 1988. Impaired pulsatile secretion of insulin in relatives of patients with non-insulin-dependent diabetes. *N. Engl. J. Med.* 318, 1225–1230.
- Ohara-Imaizumi, M., Nishiwaki, C., Kikuta, T., Nagai, S., Nakamichi, Y., Nagamatsu, S., 2004. TIRF imaging of docking and fusion of single insulin granule motion in primary rat pancreatic beta-cells: different behaviour of granule motion between normal and Goto-Kakizaki diabetic rat beta-cells. *Biochem. J.* 381, 13–18.
- Pedersen, M.G., 2009. Contributions of mathematical modeling of beta cells to the understanding of beta-cell oscillations and insulin secretion. *J. Diabetes Sci. Technol.* 3, 12–20.
- Pedersen, M.G., Sherman, A., 2009. Newcomer insulin secretory granules as a highly calcium-sensitive pool. *Proc. Natl. Acad. Sci. U.S.A.* 106, 7432–7436. doi:10.1073/pnas.0901202106.
- Pedersen, M.G., Bertram, R., Sherman, A., 2005. Intra- and inter-islet synchronization of metabolically driven insulin secretion. *Biophys. J.* 89, 107–119.
- Pedersen, M.G., Corradini, A., Toffolo, G.M., Cobelli, C., 2008. A subcellular model of glucose-stimulated pancreatic insulin secretion. *Philos. Transact. A Math. Phys. Eng. Sci.* 366, 3525–3543.
- Perez-Armendariz, M., Roy, C., Spray, D.C., Bennett, M.V., 1991. Biophysical properties of gap junctions between freshly dispersed pairs of mouse pancreatic beta cells. *Biophys. J.* 59, 76–92.
- Pisania, A., Weir, G.C., O'Neil, J.J., Omer, A., Tchipashvili, V., Lei, J., Colton, C.K., Bonner-Weir, S., 2010. Quantitative analysis of cell composition and purity of human pancreatic islet preparations. *Lab. Invest.* 90, 1661–1675. doi:10.1038/labinvest.2010.124.
- Ravier, M.A., Rutter, G.A., 2005. Glucose or insulin, but not zinc ions, inhibit glucagon secretion from mouse pancreatic alpha-cells. *Diabetes* 54, 1789–1797.
- Ravier, M.A., Guldenagel, M., Charollais, A., Gjinovci, A., Caille, D., Sohl, G., Wollenheim, C.B., Willecke, K., Henquin, J.C., Meda, P., 2005. Loss of connexin36 channels alters beta-cell coupling, islet synchronization of glucose-induced Ca²⁺ and insulin oscillations, and basal insulin release. *Diabetes* 54, 1798–1807.
- Ren, J., Sherman, A., Bertram, R., Goforth, P.B., Nunemaker, C.S., Waters, C.D., Satin, L.S., 2013. Slow oscillations of KATP conductance in mouse pancreatic islets provide support for electrical bursting driven by metabolic oscillations. *Am. J. Physiol. Endocrinol. Metab.* 305, E805–E817. doi:10.1152/ajpendo.00046.2013.
- Rhodes, C.J., 2005. Type 2 diabetes—a matter of beta-cell life and death? *Science* 307, 380–384.
- Rorsman, P., Renstrom, E., 2003. Insulin granule dynamics in pancreatic beta cells. *Diabetologia* 46, 1029–1045.
- Rorsman, P., Eliasson, L., Renstrom, E., Gromada, J., Barg, S., Gopel, S., 2000. The cell physiology of biphasic insulin secretion. *News Physiol. Sci.* 15, 72–77.
- Satin, L.S., Butler, P.C., Ha, J., Sherman, A.S., 2015. Pulsatile insulin secretion, impaired glucose tolerance and type 2 diabetes. *Mol. Aspects Med.* 42, 61–77. doi:10.1016/j.mam.2015.01.003.
- Schmitz, O., Porksen, N., Nyholm, B., Skjaerbaek, C., Butler, P.C., Veldhuis, J.D., Pincus, S.M., 1997. Disorderly and nonstationary insulin secretion in relatives of patients with NIDDM. *Am. J. Physiol.* 272, E218–E226.
- Sherman, A., 1996. Contributions of modeling to understanding stimulus-secretion coupling in pancreatic beta-cells. *Am. J. Physiol.* 271, E362–E372.

- Sherman, A., Rinzel, J., 1991. Model for synchronization of pancreatic beta-cells by gap junction coupling. *Biophys. J.* 59, 547–559.
- Sherman, A., Rinzel, J., Keizer, J., 1988. Emergence of organized bursting in clusters of pancreatic beta-cells by channel sharing. *Biophys. J.* 54, 411–425.
- Smelt, M.J., Faas, M.M., de Haan, B.J., de Vos, P., 2008. Pancreatic beta-cell purification by altering FAD and NAD(P)H metabolism. *Exp. Diabetes Res.* 2008, 165360. doi:[10.1155/2008/165360](https://doi.org/10.1155/2008/165360).
- Smolen, P., Rinzel, J., Sherman, A., 1993. Why pancreatic islets burst but single beta cells do not. The heterogeneity hypothesis. *Biophys. J.* 64, 1668–1680.
- Speier, S., Gjinovci, A., Charollais, A., Meda, P., Rupnik, M., 2007a. Cx36-mediated coupling reduces beta-cell heterogeneity, confines the stimulating glucose concentration range, and affects insulin release kinetics. *Diabetes* 56, 1078–1086.
- Speier, S., Gjinovci, A., Charollais, A., Meda, P., Rupnik, M., 2007b. Cx36-mediated coupling reduces $\{\beta\}$ -cell heterogeneity, confines the stimulating glucose concentration range, and affects insulin release kinetics. *Diabetes* 56, 1078–1086.
- Stamper, I.J., Wang, X., 2013. Mathematical modeling of insulin secretion and the role of glucose-dependent mobilization and priming of insulin granules. *J. Theor. Biol.* 318, 210–225. doi:[10.1016/j.jtbi.2012.11.002](https://doi.org/10.1016/j.jtbi.2012.11.002).
- Stamper, I.J., Jackson, E., Wang, X., 2014. Phase transitions in pancreatic islet cellular networks and implications for type-1 diabetes. *Phys. Rev. E Stat. Nonlin. Soft Matter Phys.* 89, 012719. doi:[10.1103/PhysRevE.89.012719](https://doi.org/10.1103/PhysRevE.89.012719).
- Straub, S.G., Sharp, G.W., 2002. Glucose-stimulated signaling pathways in biphasic insulin secretion. *Diabetes Metab. Res. Rev.* 18, 451–463.
- Straub, S.G., Shanmugam, G., Sharp, G.W., 2004. Stimulation of insulin release by glucose is associated with an increase in the number of docked granules in the beta-cells of rat pancreatic islets. *Diabetes* 53, 3179–3183.
- Tagliavini, A., Tabak, J., Bertram, R., Pedersen, M.G., 2016. Is bursting more effective than spiking in evoking pituitary hormone secretion? A spatiotemporal simulation study of calcium and granule dynamics. *Am. J. Physiol. Endocrinol. Metab.* 310, E515–E525. doi:[10.1152/ajpendo.00500.2015](https://doi.org/10.1152/ajpendo.00500.2015).
- van Belle, T.L., Coppelters, K.T., von Herrath, M.G., 2011. Type 1 diabetes: etiology, immunology, and therapeutic strategies. *Physiol. Rev.* 91, 79–118. doi:[10.1152/physrev.00003.2010](https://doi.org/10.1152/physrev.00003.2010).
- Wang, Z., Thurmond, D.C., 2009. Mechanisms of biphasic insulin-granule exocytosis - roles of the cytoskeleton, small GTPases and SNARE proteins. *J. Cell Sci.* 122, 893–903. doi:[10.1242/jcs.034355](https://doi.org/10.1242/jcs.034355).
- Zarkovic, M., Ceric, J., Stojanovic, M., Penezic, Z., Trbojevic, B., Dresgic, M., Nesovic, M., 1999. Effect of insulin sensitivity on pulsatile insulin secretion. *Eur. J. Endocrinol.* 141, 494–501.